Chemical Engineering Science: X 8 (2020) 100074

Contents lists available at ScienceDirect

Chemical Engineering Science: X

journal homepage: www.elsevier.com/locate/cesx

A methodology for the heuristic optimization of solvent-based CO_2 capture processes when applied to new flue gas compositions: A case study of the Chilled Ammonia Process for capture in cement plants

José-Francisco Pérez-Calvo [a], Daniel Sutter [a,1], Matteo Gazzani [b], Marco Mazzotti [a,*]

[a] Institute of Energy and Process Engineering, ETH Zurich, 8092 Zurich, Switzerland
[b] Copernicus Institute of Sustainable Development, Utrecht University, 3584 CB Utrecht, The Netherlands

ARTICLE INFO

Article history:
Received 14 April 2020
Received in revised form 15 July 2020
Accepted 19 July 2020

Keywords:
CO_2 capture
Rate-based model
Reactive absorption
Aqueous ammonia
Process optimization
Cement plants

ABSTRACT

Solvent-based post-combustion CO_2 capture technologies are key to timely decrease industrial CO_2 emissions. However, the flue gas composition differs among different industries so that different optimal operating conditions are expected. This work provides a methodology to determine the operating conditions that minimize energy consumption and maximize productivity of the capture process, for given flue gas composition and process specifications, while keeping the time required for process development at a minimal level. Firstly, it carries out a comprehensive selection and calibration of the model. Secondly, it applies a step-wise heuristic optimization procedure. In this work, this methodology has been demonstrated by means of the Chilled Ammonia Process (CAP) applied to cement plants. The optimal CAP operation has led to reboiler duties as low as 2.1 MJ_{th} $kg^{-1}_{CO_2 captured}$, while maintaining the productivity of the CO_2 absorber, thus the column height, at values similar to those typical of the power plant application.

1. Introduction

Industrial processes are responsible for 20–25% of global greenhouse gas emissions (GCCSI, 2017; International Energy Agency, 2017), with the iron and steel production and the cement industry alone responsible for more than 50% of industry-related CO_2 emissions (International Energy Agency, 2017). Approximately 25% of industrial CO_2 emissions are intrinsic to the process and can be avoided either by changing the product, thus the process, completely, or by applying CO_2 capture and storage. While the former could be preferred in the long term (yet changing steel and cement production has proved very difficult), the latter would allow to timely decarbonize such key emitters as they are. Especially for cement production, where 60% of CO_2 emissions stem from the calcination of limestone ($CaCO_3$) to produce CaO, decarbonization relies on the deployment of carbon capture and storage technologies (International Energy Agency, 2018). Among them, absorption-based post-combustion technologies are a commercial, suitable option for CO_2 capture from industrial point sources: they allow for retrofitting without affecting the industrial manufacturing process (Bui et al., 2018; Hills et al., 2016). Additionally, solvent-based CO_2 capture processes can efficiently use the waste heat available in the industrial plant for partial regeneration of the solvent and, most importantly, can use the experience acquired in their application to chemical and power plants (Ho and Wiley, 2016). There exist several commercial solutions for post-combustion capture (PCC) processes offered by, e.g., Fluor and Mitsubishi Heavy Industries (MHI) using proprietary amine solutions as solvent (Rochelle, 2016). Solvent-based processes have been extensively developed, validated and demonstrated at different scales in their application for CO_2 capture to coal- and natural gas-fired power plants (Boot-Handford et al., 2014). This includes pilot and demonstration plant projects using aqueous solutions containing monoethanolamine (MEA) (Cousins et al., 2012; Kwak et al., 2012; Mangalapally and Hasse, 2011; Notz et al., 2012; Lemaire et al., 2014; Stec et al., 2016) and mixtures with methyldiethanolamine (MDEA) (Idem et al., 2006; Sakwattanapong et al., 2005), piperazine (PZ) (Cousins et al., 2015; Rochelle et al., 2019) and mixtures with 2-amino-2-methyl-1-propanol (AMP) (Mangalapally et al., 2012; Rabensteiner et al., 2016), other amines and blends of amines (Mangalapally et al., 2012; Rabensteiner et al., 2014a; Raynal et al., 2011; Liebenthal et al., 2013; Zhang, 2013; Abu-Zahra et al., 2013), ammonia (NH_3) (Bollinger et al., 2010; Telikapalli et al., 2011; Lombardo et al., 2014; Augustsson et al., 2017), potassium carbonate (K_2CO_3) (Anderson et al., 2013; Smith et al., 2014; Anderson et al., 2014) or amino acids

* Corresponding author.
E-mail address: marco.mazzotti@ipe.mavt.ethz.ch (M. Mazzotti).
[1] Current address: Climeworks AG, Birchstrasse 155, 8050 Zurich, Switzerland.

https://doi.org/10.1016/j.cesx.2020.100074
2590-1400/

(Rabensteiner et al., 2014b; Rabensteiner et al., 2015). Furthermore, two large scale commercial plants for CO_2 capture from coal-fired power plants using solvents are in operation (Bui et al., 2018), i.e. Boundary Dam Carbon Capture Project (2020) and Petra Nova (2020).

While exhausted flue gases resulting from gas- and coal-fired power plants may contain CO_2 concentrations ranging from about 3–4 vol% (Bui et al., 2016), industrial processes generate flue gases with CO_2 concentrations between 7 and 44 vol% (Bui et al., 2016). Specifically, steel and iron manufacturing produces several gas streams with different CO_2 concentrations ranging between 5 and 30 vol% (Carpenter, 2012), while cement manufacturing produces a single flue gas stream with an average CO_2 concentration between 14 and 33 vol% (Psarras et al., 2017), depending on the plant configuration. In order to cope with the higher CO_2 concentration in the flue gas, a change in the optimal operating conditions of solvent-based capture processes is expected with respect to the application to power plants (Ho and Wiley, 2016; Andersson et al., 2016). However, solvent-based capture technologies are complex processes whose development, design and optimization following scientific criteria require: (i) detailed process model, (ii) model validation with lab and pilot experiments, (iii) sensitivity analyses, and (iv) multi-objective optimization (Abu-Zahra et al., 2016). As a consequence, techno-economic studies available in literature applying absorption-based capture processes to industrial CO_2 point sources (Hegerland et al., 2006; Barker et al., 2009; Kuramochi et al., 2012; Arasto et al., 2013; Gazzani et al., 2015; Andersson et al., 2016; Leeson et al., 2017) do not carry out a dedicated capture process design and optimization; they use instead operating conditions resulting from the optimization of solvent-based capture processes applied to gas- and coal-fired power plants (Abu-Zahra et al., 2016). There exist few simulation studies applying solvent-based post-combustion capture processes to flue gas streams containing CO_2 concentration representative of industrial processes, but these either do not use the current state-of-the-art process configuration (Tobiesen et al., 2007; Hasan et al., 2012) or do not specify how the operating conditions are identified (Dubois et al., 2017; Laribi et al., 2019). On the other hand, there is no literature discussing operating conditions for the existing industrial large-scale demonstration of CO_2 capture plants applied to: (i) steel and iron manufacturing (the Emirates Steel Indsutries (ESI) CCS Project (GCCSI, 2017)), and (ii) cement production (the pilot plant in Brevik, Norway (Bjerge and Brevik, 2014)).

In this context, this work aims at providing a methodology to optimize absorption-based post-combustion CO_2 capture processes when applied to point sources with different CO_2 concentrations in the inlet flue gas, and/or when new specifications of CO_2 capture efficiency and/or CO_2 purity are set, but reducing substantially the time required for process development, i.e. from years to, e.g. months. As a result, a set of operating conditions that minimizes the energy consumption and that maximizes the productivity of the process is selected for given input data and process specifications. This methodology requires: (i) the selection and calibration of the model using the information and data available in literature, which is shown in Section 3; and, (ii) a framework that allows for the sequential simulation and optimization of the process, which is presented in Section 4, and that starts with the simulation of the core unit, i.e. the CO_2 absorber, and that ends with the optimization of the full capture process. In order to decrease the required time, a combination of empirical choices and sound interpolations and extrapolations are included in the procedure, which at the same time tries to keep as much as possible of the rigorous approach. Notably, new experimental campaigns are avoided, relying on the information available in literature. Additionally, the application of this methodology will: (i) provide the information required for the technical evaluation and cost analysis of the solvent-based capture process in its application to the type of new point source; (ii) allow to untangle the key process features and effects of the input parameters considered; and, (iii) allow to identify opportunities for further improvement of the process and development of the model.

A case study is used to illustrate the optimization methodology proposed in this work, whose results are presented in Section 5. The development, demonstration and analysis of the method consider the application of the Chilled Ammonia Process (CAP) to cement plants. In fact, the CAP is one of the few commercial technologies for post-combustion CO_2 capture from power plants (Bollinger et al., 2010; Telikapalli et al., 2011; Lombardo et al., 2014; Augustsson et al., 2017) that has also been considered for cement application within the EU-H2020 project CEMCAP (Abanades et al., 2019). Cement manufacturing has been selected not only because of the high intrinsic CO_2 emissions associated with the process, which differs significantly from power plants, but also because of the availability of flue gas specifications. A typical European cement plant using the Best Available Technology (BAT), as defined in cooperation with the European Cement Research Academy (ECRA), generates two different flue gas compositions, one containing 18 vol% of CO_2, hereinafter referred to as "Cement Case 18", and another one containing 22 vol% of CO_2, hereinafter referred to as "Cement Case 22". A flue gas containing 14 vol% of CO_2 and generated in an ultra-supercritical (USC) pulverized coal power plant, as defined by Sutter et al. (2016), has been considered as representative of coal-fired power plants (hereinafter referred to as "Power Case"). Table 1 shows the characteristics of the flue gases considered in the case study presented in this work.

Additionally, the process specifications and constraints considered for this case study, given in Table 2, are those used by Sutter et al. (2016) when applying the CAP to the Power Case. It is worth mentioning that the CAP is always designed in this case study to avoid the formation of solids in the process; avoidance of solid formation within the packings or within other sections of the process that are not specifically designed for solid handling prevents blockages and associated operational issues.

Notably, the results of the case study here presented have been used by Voldsund et al. (2019) and Gardarsdottir et al. (2019) for the techno-economic analysis of the CAP and for the comparison with other capture technologies when applied to cement plants. Nevertheless, it is worth noting that the methodology here presented applies to different CO_2 concentrations and process specifications as well as to different solvents.

2. Solvent-based capture processes

CO_2 capture processes using aqueous amines as solvents consist of multiple sections, where CO_2, impurities and solutes are removed, recycled or reclaimed. In general, we can recognize:

(i) CO_2 capture section. This is the core part of the process. The CO_2 contained in the flue gas entering the bottom of the CO_2 absorber is transferred to the liquid flowing down countercurrently, resulting in a CO_2-depleted flue gas stream. The CO_2-lean solvent is regenerated thermally in a desorber, producing a CO_2 gas stream. Furthermore, a rich/lean countercurrent heat exchanger is used to minimize the thermal energy required in the CO_2 desorber, with a cold-rich bypass that allows for decreasing the energy required for regeneration (Lin et al., 2014) by addressing the imbalance of heat capacities between the CO_2-lean and CO_2-rich stream (Boot-Handford et al., 2014). In addition, liquid solvent intercooling and/or recycling in the CO_2 absorber are imple-

Table 1
Exhaust flue gas characteristics.

Variable	Units	Power Case	Cement Case 18	Cement Case 22
Total flowrate	[kg/s]	650	107	88
Temperature	[°C]	90	110	130
Pressure	[bar]	1.1	1.1	1.1
Composition	[mole frac.]			
y_{air}		0.738	0.730	0.670
y_{CO_2}		0.141	0.180	0.220
y_{H_2O}		0.121	0.090	0.110

Table 2
Specifications and constraints of the optimization of the CAP applied to cement plants for CO_2 capture.

Specifications	
CO_2 capture efficiency (ψ) [–]	≈ 0.9
CO_2 gas stream to compression	
Temperature [°C]	35
NH_3 concentration ($y_{NH_3}^{CO_2 comp,in}$) [ppm_v]	< 50
CO_2 purity [vol%]	> 99
Constraints	
Formation of solids	Avoided
CO_2 desorber reboiler temperature (T_{reb,CO_2}) [°C]	< 150
NH_3 concentration in the CO_2- and NH_3-depleted flue gas to acid washing [ppm_v]	< 200

mented to reduce the specific packing cost (Rochelle, 2016) as well as the energy required for solvent regeneration (Sachde and Rochelle, 2014).

(ii) Flue gas pre-conditioning section. This section serves two purposes. On the one hand, the hot flue gas is cooled down to temperatures similar to those existing at the top of the CO_2 absorber, i.e. 30–40°C (Rochelle, 2016). The temperature is typically chosen to avoid the accumulation of water in the solvent stream circulating within the CO_2 capture section. On the other hand, pretreatment of the flue gas stream is required to remove impurities that otherwise would lead to amine solvent degradation (Nwaoha et al., 2017). Flue gas treatment technologies are installed in power plants and industrial processes in order to meet regulations regarding concentration of impurities (Meuleman et al., 2016); additionally, complete removal of SO_2, inorganic chlorine compounds and fly ash can be achieved by caustic aqueous solutions (Boot-Handford et al., 2014) or by sea water scrubbing (Hegerland et al., 2006). Aqueous NH_3 solutions are able to remove not only SO_2, but also NO_2 by forming valuable by-products such as ammonium sulphate ($(NH_4)_2SO_4$) and ammonium nitrate (NH_4NO_3) salts (Meuleman et al., 2016), respectively, which avoids the formation of toxic degradation amine compounds such as nitrosamines (Boot-Handford et al., 2014; Reynolds et al., 2016).

(iii) CO_2 water-wash (CO_2-WW) section. Gaseous amine losses exiting the CO_2 desorber are limited by means of a direct contact cooler (DCC) using a liquid water stream flowing in counter-current with the CO_2 gaseous stream.

(iv) CO_2 compression section. The purified CO_2 gas stream is compressed to supercritical conditions to meet the specifications required for transportation and storage.

(v) Flue gas water-wash (FG-WW) section. The CO_2-depleted flue gas exiting the CO_2 absorber might contain significant amounts of amine solvent, depending on the amine partial pressure at typical operating conditions found at the CO_2 absorber top (Nguyen et al., 2010). Additionally, it might contain significant concentration of volatile compounds, such as organic acids or NH_3, resulting from the oxidative degradation of the amine at CO_2 absorber conditions (Gouedard et al., 2012; Mazari et al., 2015) or from the NH_3 solution itself. Therefore, this stream is further treated in a flue gas water-wash section, which generally consists of a water-based absorption unit.

(vi) Recovery section. Heavy compounds are generated by thermal degradation of the amine (referred to as amine degradation heavy compounds (ADHC) hereinafter) at CO_2 desorber conditions, while heat stable salts (HSS) accumulate in the solvent due to the dissolution of acidic compounds from the flue gas, i.e. SO_2 and NO_2. Therefore, a slipstream is purged from the CO_2 absorption–desorption main loop to avoid the accumulation of ADHC and HSS in the solvent (Reynolds et al., 2016; Nwaoha et al., 2017). Thermal reclamation allows for the recuperation of amine solvent and captured CO_2 from the purged stream, which is recycled to the CO_2 capture section and thus decreases the flowrate of fresh amine make-up (Kentish, 2016).

(vii) Flue gas heating section. The need for such section depends on local regulations and environmental constraints, and on the temperature of the flue gas exiting the FG-WW section. In general, a direct contact heater (DCH) is utilized to increase the temperature of the clean CO_2-depleted flue gas before reaching the stack: this is required to achieve a wide spread of the vapour plume. In the DCH, the water heated up in the flue gas pre-conditioning section is used flowing counter-currently with the clean flue gas. This heat integration allows for decreasing the cooling demand as well as the flowrate of purged water.

The seven sections described above are evident in the CAP, whose process flow diagram (PFD) is shown in Fig. 1. The main additional complexity of the CAP stems from the high volatility of the solvent, and thus from the necessity of limiting and controlling NH_3 losses and emissions. Therefore, the CAP requires some adaptations with respect to general amine-based CO_2 capture processes, as follows:

- A slip stream of the cold CO_2-rich stream, the so-called absorber pumparound, is cooled, chilled and sent to the top of the CO_2 absorber in order to minimize the NH_3 slip to the gas. The lower the temperature and the higher the CO_2 loading in the pumparound, the lower the equilibrium partial pressure of NH_3 thus the NH_3 concentration in the CO_2-depleted flue gas leaving the CO_2 absorber. However, a minimum temperature exists for each pumparound composition in order to avoid solid formation (Sutter et al., 2015).
- Differently to amines, the amount of NH_3 contained in the CO_2-depleted flue gas entering the NH_3 absorber can reach concentrations as high as 2,000 to 15,000 ppm_v (Sutter et al., 2016). Therefore, the FG-WW section not only consists of an absorber, but it also requires a desorption unit in order to minimize solvent and CO_2 losses. The gas stream leaving the top of the NH_3 desorber, which is rich in CO_2 and NH_3 is recycled to the

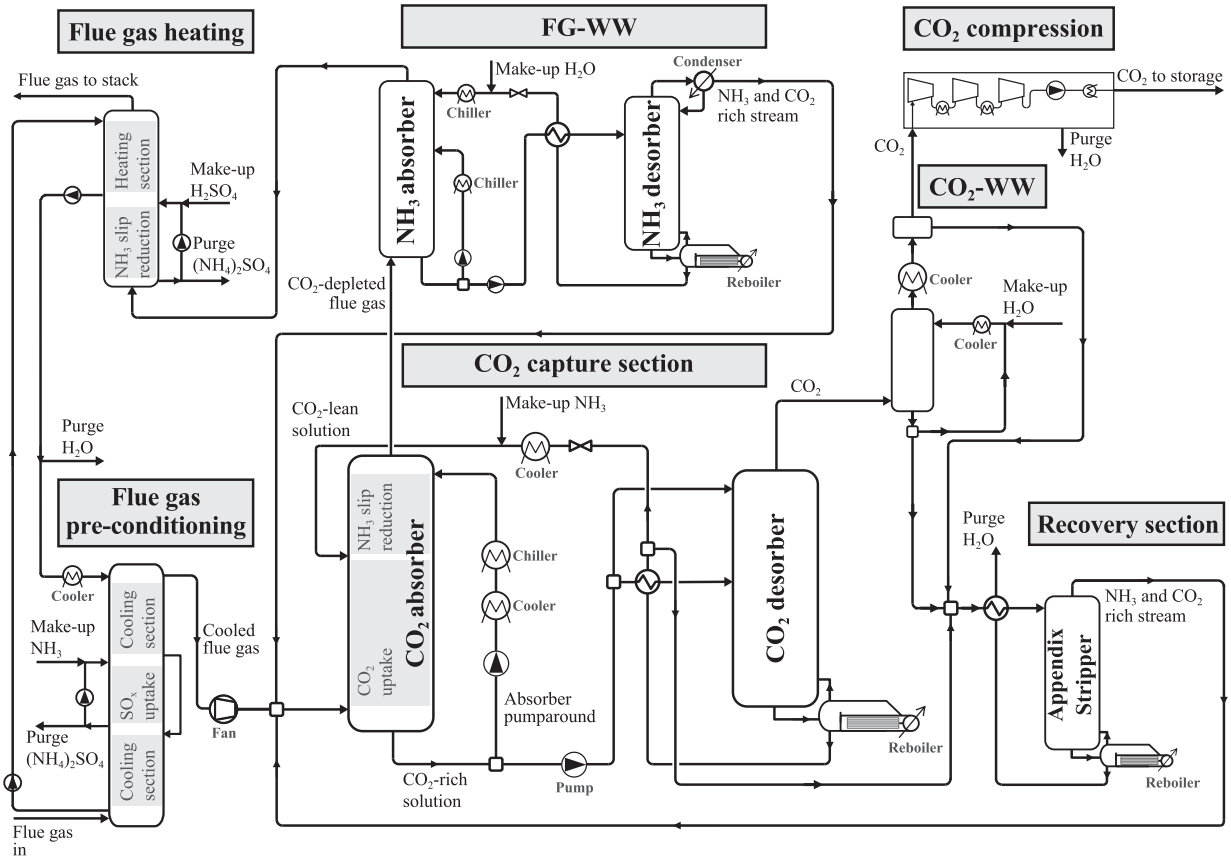

Fig. 1. Process Flow Diagram (PFD) of the CAP.

bottom of the CO_2 absorber; the liquid stream leaving the bottom of the NH_3 desorber is mainly composed of water and is recycled, after cooling and chilling, to the top of the NH_3 absorber.

- While both amine- and NH_3-based processes require that part of the lean cold liquid is purged, in the case of the latter this is a consequence of the accumulation of water within the system (Yu and Wang, 2015): The temperature of the flue gas exiting the NH_3 absorber is lower than the temperature of the flue gas entering the CO_2 absorber. To avoid the loss of NH_3 and CO_2, the purged stream is sent to an appendix stripper. The appendix stripper is designed to recover more than 99.8% of apparent NH_3 at the top of the column (and all CO_2), which is sent back to the bottom of the CO_2 absorber. As a result, a water stream containing less than 150 ppm_{wt} NH_3 is obtained at the bottom of the appendix stripper, which is purged to close the water balance within the process. Notably, the appendix stripper also avoids the accumulation of acidic compounds in the liquid solvent.
- The flue gas exiting the NH_3 absorber contains up to 200 ppm_v of NH_3. Therefore, an acid-wash using an aqueous solution of sulfuric acid (H_2SO_4) is placed before the DCH to keep NH_3 emissions within emission limits. As a consequence, $(NH_4)_2SO_4$ is produced.

Clearly, the CAP shares both the process layout and many of the issues that most promising amine solutions possess (e.g. solvent volatility as for AMP (Sutter et al., 2016; Nguyen et al., 2010), and solid formation as for piperazine (Freeman et al., 2010; Brúder et al., 2011)). Therefore, we are convinced that the methodology presented in this work can be fully applied to other amine solvents.

3. Model selection, development and validation

Solvent-based CO_2 capture processes can be described using detailed mathematical models; therefore, process simulation software is a convenient and suitable tool for the rigorous simulation of such complex processes.

An accurate and reliable model is of paramount importance when performing process simulation and optimization. Energy consumption, column sizing and process feasibility regions are drastically influenced by the capability of the model to reproduce the underpinning physics and chemistry. More specifically, the detailed design of the CO_2 absorber requires the use of rate-based process simulations that consider material and energy transfer limitations between the vapour and the liquid phase. The rate version of Aspen Plus' RadFrac model (RateSep), which is broadly regarded as an accurate tool both in academia and industry, has been used in this work to simulate the CO_2 absorption packed column. Aspen RateSep applies the Maxwell–Stefan theory to describe mass transfer for each component. The column is discretized along its axial direction and separate balances are considered for each phase, which consists of a bulk and a film section in contact with the other phase's film. Average bulk conditions are considered for each axially discretized volume in each phase, with different options available for averaging. Equilibrium between the liquid and the vapour phases is imposed at the interface, and mass and heat transfer resistances are computed by means of the two-film theory. Non-linear profiles are reconstructed by radial discretization within the films. Numerical options are available in Aspen RateSep to set the column and film discretization modes, and to compute the properties of the bulk phases in each axial segment (referred to as "flow model" in Aspen RateSep). The computation

of the driving force required for mass transfer is obtained by means of the thermodynamic model, and the computation of the mass and heat transfer resistances takes into account the kinetically-controlled chemical reactions. The column hydrodynamics are considered by means of correlations used for the computation of the mass and heat transfer coefficients, the vapour-liquid interfacial area, liquid hold-up and pressure drop. Models for the computation of transport properties required in the aforementioned correlations are used. For a more detailed description of Aspen RateSep, the interested reader is referred to comprehensive works available in the literature on this topic (Zhang et al., 2009; Liu et al., 2015).

Accordingly, the starting point to optimize a PCC process is a reliable rate-based model validated experimentally. A critical analysis of models available in the literature is crucial to assess their applicability to the new conditions, and to identify inconsistencies and opportunities for improvement. Specifically, here we started from the work of Qi et al. (2013), which provides a rate-based model for the CO_2-NH_3-H_2O system that has been validated using the CO_2 absorption pilot tests reported by Yu et al. (2011). However, opportunities for the improvement of the model have been identified, and subsequently, the model has been tuned to make it more physically sound and suitable for process optimization at typical operating conditions of the CO_2 absorber. If not stated otherwise, options specified in the rate-based model of Qi et al. (2013) have been selected for this work.

3.1. Thermodynamic model

Generally, thermodynamic models used in solvent-based CO_2 capture processes are validated with VLE, liquid speciation and heat of absorption experimental data at typical operating conditions of the capture process. Specifically for the CO_2-NH_3-H_2O system, Qi et al. (2013) selected the thermodynamic model developed by Que and Chen (2011) (referred to as "Chen model" hereinafter), which uses the electrolyte NRTL model for the computation of activity coefficients in the liquid phase and the Redlich-Kwong equation of state for the fugacity coefficients in the vapour phase. While the Chen model has been proven to reproduce the VLE experimental data (Qi et al., 2013), it considers the formation of ammonium bicarbonate (NH_4HCO_3) as only solid. On the contrary, experiments in the literature have shown that other solid compounds form, e.g. ammonium sesqui-carbonate ($(NH_4)_2CO_3{\cdot}2NH_4HCO_3$), ammonium carbonate monohydrate ($(NH_4)_2CO_3{\cdot}H_2O$) and ammonium carbamate (NH_2COONH_4) (Jänecke, 1929a; Jänecke, 1929b). In this regard, the thermodynamic model proposed by Thomsen and Rasmussen (1999) and further developed by Darde et al. (2010) (referred to as "Thomsen model" hereinafter) has been proven to describe accurately experimental SLE data, making it suitable to predict criticalities within the CAP regarding solid formation (Sutter et al., 2015). In addition, the Thomsen model outperforms the Chen model in reproducing the experimental VLE data available in literature (Darde et al., 2012). Consequently, the Thomsen model has been selected in the case study shown in this work. It uses the extended UNIQUAC equation for the computation of the activity coefficients in the liquid phase, the Redlich-Kwong-Soave equation of state for the computation of the gas-phase fugacity coefficients and assumes activity coefficient equals 1 for the pure solids that can be formed.

3.2. Liquid phase reaction kinetics

Chemical reactions taking place in the aqueous amine solution enhances CO_2 absorption capacity. On the one hand, there exist instantaneous reactions that involve the transfer of a proton. On the other hand, dissolved CO_2 can react with OH^- to form the bicarbonate ion (HCO_3^-). In addition, primary and secondary amines react with CO_2 to form the carbamate ion. These two reaction types are kinetically controlled reactions (Puxty and Maeder, 2016). CO_2 absorption into aqueous NH_3 solutions follows the same liquid-phase reaction scheme as primary amines.

$$H_2O(l) \overset{K_1}{\rightleftharpoons} H^+ + OH^- \tag{1}$$

$$H_2O(l) + NH_3(aq) \overset{K_2}{\rightleftharpoons} NH_4^+ + OH^- \tag{2}$$

$$HCO_3^- \overset{K_3}{\rightleftharpoons} H^+ + CO_3^{2-} \tag{3}$$

$$CO_2(aq) + OH^- \underset{k_{-4}}{\overset{k_{+4}}{\rightleftharpoons}} HCO_3^- \tag{4}$$

$$CO_2(aq) + NH_3(aq) \underset{k_{-5}}{\overset{k_{+5}}{\rightleftharpoons}} NH_2COO^- + H^+ \tag{5}$$

Therefore, the CO_2 absorption rate into the liquid solution is determined by the reaction rate of CO_2 with OH^- to form HCO_3^-, and of CO_2 with NH_3 to form NH_2COO^-, or with the amine in the case of primary amines and some secondary amines. In the case of NH_3, primary amines and some secondary amines, the reaction with CO_2 to form the carbamate ion has been reported to have a predominant effect on the CO_2 absorption rate at typical operating conditions of the capture process (Puxty and Maeder, 2016; Jilvero et al., 2014); an accurate forward reaction rate of reaction (5) is of paramount importance for realistic modelling of the CO_2 absorber. Two different mechanisms have been proposed for the reaction of amine with CO_2 to form the carbamate ion: (i) via the formation of a zwitterion followed by its deprotonation (Caplow et al., 1968; Danckwerts, 1979); and, (ii) via a termolecular mechanism (Crooks and Donnellan, 1989; Da Silva and Svendsen, 2004). Additionally, an elementary reaction kinetic model is proposed in the case of NH_3 (Wang et al., 2011). The experimental techniques used for the determination of the reaction kinetics measure either the gas–liquid mass transfer rates of CO_2 into the solvent, or the reaction rate of CO_2 after rapid mixing of liquid phases containing the reactants (Vaidya and Kenig, 2007; Couchaux et al., 2014). While the former -heterogeneous techniques- require the modelling of mass transfer, the latter -homogeneous techniques- can only be applied at very dilute concentrations that allow for the detection of concentration changes over time. In general, kinetic models obtained at operating conditions typical of the CO_2 capture process by means of heterogeneous techniques outperform those kinetic models obtained at dilute concentrations, regardless of the reaction mechanism assumed, as shown in the literature for MEA (Amirkhosrow et al., 2020). However, NH_3 may undergo significant evaporation when the reaction kinetics are determined for liquid compositions typical of the industrial capture process (Kim et al., 2014), thus making the measurement inaccurate. As a consequence, significantly different values of the apparent kinetic constant for the reaction of CO_2 with NH_3 have been obtained by different authors (Darde et al., 2011; Yu et al., 2016; Lillia et al., 2018). Out of them, only the kinetic model proposed by Pinsent et al. (1956a) has been successful when implemented in a rate-based model to reproduce pilot test results for CO_2 capture with aqueous NH_3 solutions (Qi et al., 2013). Notably, the kinetic model of Pinsent et al. (1956a) has been obtained by means of homogeneous techniques mixing very dilute aqueous solutions of the reactants. Similar kinetic parameters to those of Pinsent et al. were obtained by Wang et al. (2011) for the reaction of CO_2 with NH_3, using the same type of experimental approach. As for the reaction mechanism of the bicarbonate ion formation reaction, it is interpreted in the literature as an elementary reaction; similar reaction rate constants have been obtained by different authors when

accounting for the ionic strength of the solution (Kucka et al., 2002), including the kinetic model of Pinsent et al. (1956b) that used the same experimental technique as for the reaction with NH_3.

Therefore, the forward reaction rate of reaction (4) and (5) have been modelled within the case study of this work using the reaction kinetics obtained by Pinsent et al. (1956a, 1956b), (referred to as "Pinsent model" hereinafter) using the following power law reaction rate expressions:

$$r_{+4} = k_{0,+4}^{(c)} \exp\left(\frac{-E_{+4}^{(c)}}{RT}\right) c_{CO_2} c_{OH^-} \tag{6}$$

$$r_{+5} = k_{0,+5}^{(c)} \exp\left(\frac{-E_{+5}^{(c)}}{RT}\right) c_{CO_2} c_{NH_3} \tag{7}$$

where $k_{0,+j}^{(c)}$ is the pre-exponential factor and $E_{+j}^{(c)}$ is the activation energy of the concentration-based reaction rate constants in the Pinsent model, with j referring either to the forward reaction (4) (Pinsent et al., 1956b) or to the forward reaction (5) (Pinsent et al., 1956a). Nevertheless, the Pinsent model has some limitations. On the one hand, reaction rate constants are function not only of temperature, but also of composition in the case of non-ideal chemical solutions (Froment and Bischoff, 1990). However, reaction rate constants in the Pinsent model are estimated from very dilute solutions, e.g. with NH_3 concentrations between 0.027 and 0.19 M (Pinsent et al., 1956a), which are far from the more concentrated solutions expected within the capture process. On the other hand, the Pinsent model only provides the reaction rate of the forward reactions, while especially the backward reaction of (5) might be significant at compositions of the CO_2-rich stream in the capture process (Astarita, 1967). The model can therefore be improved by adopting activity-based reaction kinetics, which allow: (i) to introduce the effect of composition on the reaction rate constant, thus enabling the extrapolation of the kinetic model at higher NH_3 and CO_2 concentrations in the liquid phase; and, (ii) to compute the reaction rate for the backward reactions of (4) and (5) assuming microscopic reversibility (Masel, 2001). The activity-based reaction rates of the forward reactions of (4) and (5) are expressed as follows:

$$r_{+4} = k_{0,+4}^{(a)} \exp\left(\frac{-E_{+4}^{(a)}}{RT}\right) \gamma_{CO_2}^{*} \gamma_{OH^-}^{*} x_{CO_2} x_{OH^-} \tag{8}$$

$$r_{+5} = k_{0,+5}^{(a)} \exp\left(\frac{-E_{+5}^{(a)}}{RT}\right) \gamma_{CO_2}^{*} \gamma_{NH_3}^{*} x_{CO_2} x_{NH_3} \tag{9}$$

where $k_{0,+j}^{(a)}$ is the pre-exponential factor and $E_{+j}^{(a)}$ is the activation energy of the activity-based reaction rate constants, with j referring to the forward reaction (4) or to the forward reaction (5), and γ_i^* and x_i are the rational, unsymmetrical activity coefficient and the molar fraction, respectively, of species i.

The activity-based reaction rate constants of the forward reaction of (4) and (5) are computed from the concentration-based reaction rate constants reported in Pinsent model, $k_{+4}^{(c)}$ (Pinsent et al., 1956b) and $k_{+5}^{(c)}$ (Pinsent et al., 1956a), obtained at infinite dilution conditions, as follows:

$$k_{+4}^{(a)} = k_{+4}^{(c)} \rho_w^2 \tag{10}$$

$$k_{+5}^{(a)} = k_{+5}^{(c)} \rho_w^2 \tag{11}$$

where ρ_w is the molar density of pure water, which is a function of temperature. The conversion strategy from concentration- to activity-based kinetics is similar to that proposed in the literature for aqueous MEA solutions (Zhang et al., 2009), although in the case of aqueous NH_3 solutions the conversion has been carried out at infinite dilution due to the lack of reliable kinetics obtained at concentrations typical of the capture process. On the contrary, our conversion approach is different than that implemented by Qi et al. (2013) for the CO_2-NH_3-H_2O system, who instead used the Pinsent model reaction rate constants obtained at infinite dilution to generate reaction rate values at greater concentrations, which were then used for the determination of the activity-based reaction rate constants.

The activity-based reaction rates of the backward reaction of (4) and (5) assuming microscopic reversibility can be expressed, respectively, as:

$$r_{-4} = k_{0,-4}^{(a)} \exp\left(\frac{-E_{-4}^{(a)}}{RT}\right) \gamma_{HCO_3^-}^{*} x_{HCO_3^-} \tag{12}$$

$$r_{-5} = k_{0,-5}^{(a)} \exp\left(\frac{-E_{-5}^{(a)}}{RT}\right) \gamma_{NH_2COO^-}^{*} \gamma_{H^+}^{*} x_{NH_2COO^-} x_{H^+} \tag{13}$$

where the activity-based backward reaction rate constants can be computed from the concentration-based forward reaction rate constants reported in literature and obtained at infinite dilution, and from the reaction equilibrium constants, K_4 and K_5, computed assuming pure water and solutes at infinite dilution as reference state:

$$k_{-4}^{(a)} = \frac{k_{+4}^{(c)} \rho_w^2}{K_4} \tag{14}$$

$$k_{-5}^{(a)} = \frac{k_{+5}^{(c)} \rho_w^2}{K_5} \tag{15}$$

As a result, the kinetic parameters $k_{0,+j}^{(a)}, k_{0,-j}^{(a)}, E_{+j}^{(a)}$ and $E_{-j}^{(a)}$ have been estimated in this work for temperatures between 0 and 50°C, departing from the concentration-based forward reaction rate constants reported in the Pinsent model (Pinsent et al., 1956a; Pinsent et al., 1956b) and using the value of the equilibrium constants considered in the Thomsen model (Darde et al., 2010). The resulting parameters are reported in Table 3.

3.3. Liquid density and transport property models

Liquid solvent density and transport properties affect the hydrodynamic conditions within the CO_2 absorber. Specifically, the accurate determination of density, viscosity, surface tension and thermal conductivity of the liquid phase, as well as of the diffusivity of the individual components within the liquid phase is of paramount importance for proper heat and mass transfer determination (Zhang et al., 2009; Liu et al., 2015).

The transport property models implemented by Qi et al. (2013) for the CO_2-NH_3-H_2O system have been selected in this work. Nevertheless, such models were only validated for unloaded solvent mixtures, i.e. NH_3-H_2O mixtures, without considering dissolved CO_2. Therefore, we have added available literature data for liquid ternary mixtures of CO_2-NH_3-H_2O and for liquid binary mixtures of CO_2-H_2O to adjust the parameters of the transport property models of liquid ternary CO_2-NH_3-H_2O mixtures. Specifically, we have estimated the model parameters for the computation of liquid density and viscosity, and selected new literature parameter values for liquid viscosity and diffusivity computations. The new values of the model parameters, as well as the validation of the updated transport property models and the description of the models can be found in the Supplementary Material.

Table 3
Kinetic parameters for the computation of the reaction rate of the forward and backward reactions given by reaction (4) and reaction (5).

Reaction	$k_j^{(a)}$ [kmol/(m^3 s)]	$E_j^{(a)}$ [kJ/kmol]
+4	1.059×10^{17}	54933
+5	3.308×10^{14}	47963
−4	1.094×10^{16}	102757
−5	6.194×10^{21}	56173

3.4. Numerical options

The approach adopted for the axial discretization of the column, i.e. flow model and discretization grid, affects the results, the computational convergence of the unit and the computational time, e.g. a finer axial discretization grid improves the precision of the simulation, but increases the computational time. A compromise has been found with a length per segment of 0.1 m using Vplug as flow model in RateSep, whose selection has taken into account literature studies applying comprehensive sensitivity analyses (Zhang et al., 2009; Liu et al., 2015; Amirkhosrow et al., 2020). Vplug considers the conditions of the liquid bulk phase at each stage to be equal to the outlet conditions, while the conditions of the vapour bulk phase in each stage are averaged between inlet and outlet conditions. When the length of the axial segments is small enough, the flow model has a negligible influence on the simulation results.

While concentration profiles within the vapour film can be assumed to be linear due to the absence of chemical reactions, the physical mass transfer of CO_2 from the vapour-liquid interface to the liquid bulk will be enhanced by chemical reactions, leading to a non-linear decay of the concentration of CO_2. With the aim of describing such concentration profiles within the liquid film, and thus of better approximating the mass and energy transfer from the vapour to the liquid phase, the discretization of the liquid film is required. RateSep provides several options for the discretization of the film, including equidistant and different asymmetrical grid distributions. Asymmetrical grid distributions allow for smaller film segments closer to the vapour-liquid interface, which is preferred in order to describe the steeper CO_2 concentration decay in that region of the liquid film at typical CO_2 absorber conditions. In this work, we adopt the so-called geometric discretization of the liquid film, whereby the ratio α is defined as:

$$\alpha = \frac{x_{i+1} - x_i}{x_i - x_{i-1}} \tag{16}$$

where x_i is the discretization point, with $x_0 = 0$ at the interface and $x_n = \delta$ defines the film thickness. We define $\alpha > 1$ in order to have a discretization grid finer next to the liquid–vapour interface. Then, Eq. 16 can be written as a second order difference equation, as follows:

$$x_{i+1} - (1 + \alpha)x_i + \alpha x_{i-1} = 0 \tag{17}$$

Its solution for $i = 0, \ldots, n$ is:

$$\frac{x_i}{\delta} = \frac{\alpha^i - 1}{\alpha^n - 1} \tag{18}$$

The discretization of the liquid film affects significantly the accuracy of the model and the time required for the computations, with contrasting effects. The thorough selection of the suitable number of segments and discretization ratio requires a time demanding approach consisting of several process simulations and numerical validation with respect to literature experimental results (Zhang et al., 2009; Amirkhosrow et al., 2020). Here, we propose the selection of the liquid film discretization via a physical analysis of the reactive absorption process within the liquid film that allows for a faster and more general approach. Specifically, we have used the approach proposed by Asprion (2006), adapted to the film discretization approach described by Eq. (18). In order to reproduce accurately the steep CO_2 concentration decay taking place next to the liquid–vapour interface, Asprion proposes that half of the liquid film segments are contained within the chemical film thickness, δ_{chem}, which is the thickness of the diffusive liquid film where chemical reactions enhance CO_2 mass transfer, such that:

$$\delta_{chem} = x_{n/2} \tag{19}$$

On the one hand, the thickness of the liquid film, δ, is computed by RateSep as the ratio of the average diffusivity, D, and the average physical mass transfer coefficient, k (Aspen Technology Inc., 2014):

$$\delta = \frac{D}{k} \tag{20}$$

On the other hand, δ_{chem} can be estimated as the ratio between D and the mass transfer coefficient in the liquid phase enhanced by chemical reaction, $k\prime$:

$$\delta_{chem} = \frac{D}{k\prime} = \frac{D}{Ek} \tag{21}$$

where E is the enhancement factor, i.e. the ratio between the uptake rate of CO_2 when reactions occur in the liquid phase and the uptake rate of CO_2 if only physical mass transfer takes place. Therefore, the decrease of the thickness of the diffusive liquid film when chemical reaction takes place with respect to the case in which there is only physical absorption depends on the value of E, i.e.:

$$\frac{\delta_{chem}}{\delta} = \frac{1}{\mathrm{E}} \tag{22}$$

Considering Eqs. (18), (19) and (22), we obtain an expression that allows to determine the film discretization ratio, α, as a function of the number of segments within the liquid film, n, depending on the physicochemical properties of the reactive absorption process, which are represented by the value of E.

$$\alpha^n - \mathrm{E}\,\alpha^{\frac{n}{2}} + \mathrm{E} - 1 = 0 \tag{23}$$

For a coarse grid, an increase in the number of segments within the liquid film modifies the mass transfer results obtained. As soon as the grid becomes fine enough, increasing the number of segments of the liquid film does not change the results. On the contrary, increasing the number of segments leads to a steady increase in the computational time. For the CAP, a trade-off was found when defining 7 discretization segments within the liquid film, leading to simulations of the CO_2 absorber lasting between 20 and 40 s (Intel® Core™ i5-8500 CPU @ 3.40 GHz). Additionally, we can assume that amine in the liquid is in large excess with respect to dissolved CO_2 at typical operating conditions of the absorber in CO_2 capture processes. Consequently, the amine concentration drop within the liquid film can be neglected. In that case, pseudo-first order kinetics with respect to CO_2 concentration can be assumed and the value of the enhancement factor equals the Hatta number, Ha (Levenspiel, 1999). If the reaction of CO_2 with OH^- is neglected -assuming that the consumption of CO_2 within the liquid film is mainly due to its reaction with the amine, or with NH_3 in this case study-, the Hatta number can be computed as:

$$\mathrm{Ha} = \frac{\sqrt{k_{+5}^{(c)} c_{NH_3} D_{CO_2,L}}}{k_{l,CO_2}^0} \tag{24}$$

where $D_{CO_2,L}$ is the diffusivity of CO_2 in the liquid and k_{l,CO_2}^0 is the physical mass transfer coefficient for CO_2. In this work, the operating conditions for CO_2 capture lead to values of Ha that vary approx-

imately between 3 and 30. If the liquid film is divided into 7 segments, a film discretization ratio between 1.2 and 2.6 is obtained by means of Eq. (23) for Ha between 3 and 30, respectively. Therefore, an intermediate value of 1.5 has been selected. The numerical options of the liquid film discretization selected for this case study are similar to those proposed by Amirkhosrow et al. (2020) resulting from a more time consuming numerical validation using pilot plant experimental results; their study applies to MEA as solvent instead, but the values of Ha are similar to those computed in this work for the CAP.

3.5. Model validation

Models have to be validated using the results of pilot plant tests. Pilot tests in a packed-bed absorption column at typical industrial operating conditions are required in order to guarantee the prediction capabilities of the model when scaling-up. For example, the tests of Notz et al. (2012) are broadly used in literature studies to validate rate-based models using MEA as solvent (Kale et al., 2013; Li et al., 2016; Luo and Wang, 2017; Amirkhosrow et al., 2020).

In the case of aqueous NH_3 solutions for CO_2 capture, pilot test results have been reported by Yu et al. (2011) and further detailed by Qi et al. (2013), and have been used in this work for the validation of the rate-based model developed for our case study. The pilot plant CO_2 absorber contains a random packing of 25-mm Pall rings with a specific surface area of 207 m^2m^{-3}. Correlations for the computation of the mass and heat transfer coefficients, of the effective interfacial area between the liquid and the vapour phase and of the liquid hold-up within the column are available in Aspen Plus, Version 8.6. Different combinations of these correlations, together with the building blocks of the model and the numerical options selected before, have been tested. As a result of this comprehensive assessment, mass transfer coefficients and interfacial area are computed by the correlation of Onda et al. (1968), energy transfer coefficients are computed by means of the Chilton and Colburn analogy (Chilton and Colburn, 1934), and liquid hold-up using the model of Stichlmair et al. (1989). The rate-based simulation of the CO_2 absorber is initialized using an initial liquid hold-up per stage ranging from 0.01 to 0.1% of the total stage volume. The rate-based model validation results are shown in Fig. 2.

In general, the rate-based model is able to reproduce the experimental values with an error below 20%, while also matching the experimental temperature profiles along the absorption column. The model features described above, e.g. including the composition effects in the rate constants, and the results shown in Fig. 2 make the rate-based model presented in this work suitable for process simulation and optimization applied to flue gases with higher CO_2 concentration.

It is worth noting that our optimization methodology proposes equilibrium-based simulations of the CO_2 desorber, since rate-based simulations would increase simulation times considerably without improving the accuracy significantly. This is justified by the faster transport phenomena and reaction kinetics at high temperatures such as those typical of the CO_2 desorber (Zhang et al., 2009), which typically range between 80°C or above at the top of the column and 150°C at the reboiler. In fact, equilibrium-based simulations of the CO_2 desorber have been reported to reproduce the experimental column profiles regarding CO_2 concentration in the gas phase and temperature, as well as the experimental values reported for the reboiler duty -as long as the rate-based simulation of the CO_2 absorber is able to provide accurate results for the inlet streams to the desorber (Zhang and Chen, 2013). Therefore, our optimization methodology does not consider the validation of the rate-based model at high temperatures, and the simulation of the CO_2 desorber relies on the accuracy of the thermodynamic model in predicting the V-L equilibrium (see Section 3.1). Still, such validation could be carried out as described for the CO_2 absorber, provided that pilot plant experimental results for the CO_2 desorber are available, at the cost of longer process development.

4. Sequential process optimization procedure

The goal of our optimization procedure is to determine the operating conditions that minimize energy consumption and maximize productivity of the capture process, for a given CO_2 concentration in the inlet flue gas and specified values of CO_2 capture efficiency and CO_2 purity. Finding the solution of such an optimization problem faces two main challenges: (i) computation times for the rate-based simulation of the full process are of the order of hours; and, (ii) the knowledge of a feasible initial point, i.e. a set of operating conditions and sizes of equipment, is needed.

The procedure developed here to solve the optimization problem and to overcome its challenges is based on two elements:

- The availability of a reference optimized design (from literature) for a post-combustion CO_2 capture process, designed for a different CO_2 concentration in the flue gas and/or for a different specified value of the CO_2 capture efficiency. The information about operating conditions, Murphree efficiencies at those conditions, and the understanding of which among the many parameters are critical for the process performance must be available for the reference design.
- The possibility of using not only a rate-based model but also an equilibrium-based model (whose simulation of the full capture process takes minutes instead of hours), whereby the Murphree efficiencies can be tuned by using the rate-based model.

In practice, our optimization procedure consists of three main steps, which are illustrated in Fig. 3 and described below.

Step 1. Determination of a feasible set of operating conditions of the CO_2 absorber, which is used as initial condition for the optimization of the capture process applied to the new case.

Firstly, the values of the CO_2 absorber decision variables are manually adapted to fulfil the specifications and constraints of the new case, starting from the optimal set of operating conditions of the CO_2 absorber of the reference case. At this stage, equilibrium-based simulations of the stand-alone CO_2 absorber using the Murphree efficiency values of the reference case are applied to the new case. Such adaptation of absorber parameters is based on the previous know-how of the capture process and on the knowledge of the effect of the CO_2 decision variables on the performance of the column. The **CO_2 absorber decision variables**, which affect significantly both the energy performance and the productivity of the process, are:

- Apparent solvent concentration, $\hat{c}_{solvent}$ [$mol_{solvent}$ $kg^{-1}_{H_2O}$].
- CO_2 loading of the CO_2-lean stream, l_{lean} [mol_{CO_2} $mol^{-1}_{solvent}$], which is the ratio between the apparent moles of CO_2 and the apparent moles of solvent in the CO_2-lean stream entering the CO_2 absorber.
- Liquid-to-gas flowrate ratio for the CO_2-lean liquid and inlet gas streams entering the CO_2 absorber, L^{lean}/G^{in} [kg kg^{-1}].
- Pumparound and/or intercooling temperature, T_{pa} [°C].
- Pumparound and/or intercooling split fraction, f_s [–].

Secondly, the CO_2 absorber with the feasible operating conditions applied to the new case is simulated using the rate-based model, resulting in the determination of the dimensions of the packing section, i.e. length and diameter, that meet the separation performance, i.e. CO_2 capture efficiency and solvent losses, of the

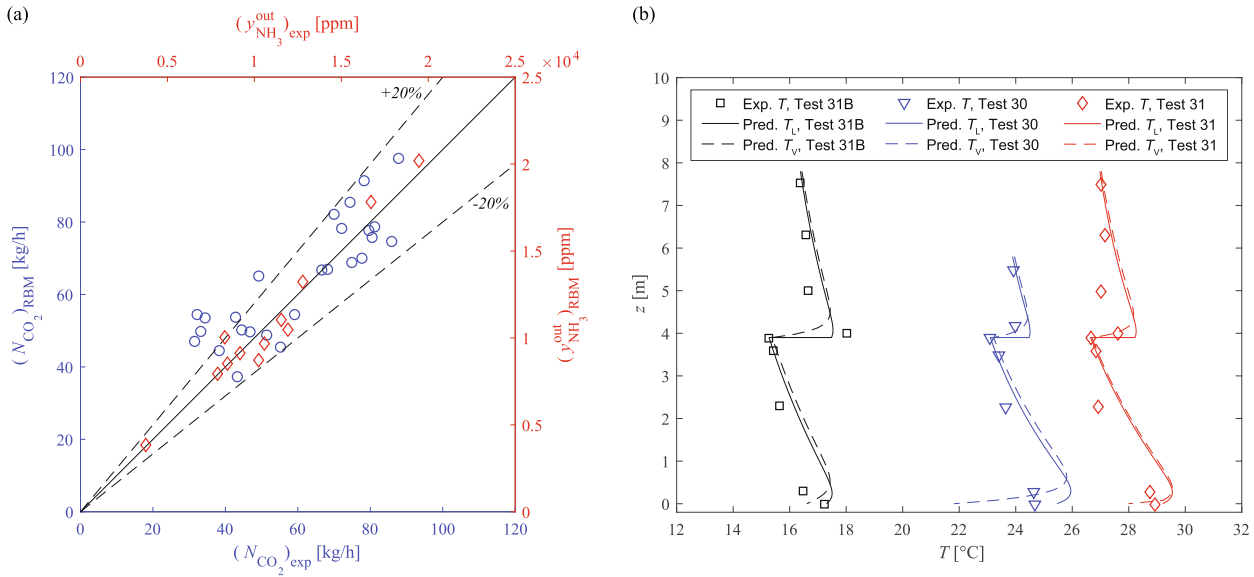

Fig. 2. Validation of the rate-based model developed in this work with the CO_2 absorber pilot plant test results reported in literature (Yu et al., 2011; Qi et al., 2013). (a) Parity plots showing the prediction of the model (RBM) vs. the experimental results (exp) of the CO_2 absorption rate, N_{CO_2}, (◯) and the NH_3 concentration in the CO_2-depleted flue gas exiting the column, $y^{out}_{NH_3}$, (◇); the parity line (—) and lines showing 20% deviation with respect to the parity line (– –) are shown. (b) Experimental temperature profile along the CO_2 absorber for three different tests, i.e. 31B (□), 30 (▽) and 31 (◇), and prediction of the model for the liquid phase, L, (—) and the vapour ph.ase, V (– –).

previous equilibrium-based simulation. Subsequently, new Murphree efficiency values are computed for the new case, and implemented in the equilibrium-based model of the CO_2 absorber. The new Murphree efficiency values of the CO_2 absorber obtained for the feasible set of operating conditions of the new case are adopted from now on when performing equilibrium-based simulations of the column.

Thirdly, a first full process equilibrium-based simulation for the new case is carried out using the feasible set of operating conditions found previously. Subsequently, single variable sensitivity analyses are performed to study the influence of the process operating variables on: (i) the energy demand, (ii) the fulfilment of the specifications and constraints of the capture process, and (iii) the convergence stability of the process simulation. As a result and using also the previous know-how of the process, we determine: (i) the process decision variables whose value has to be modified to optimize the capture process, (ii) feasible ranges for the process decision variables, and (iii) the process parameters that do not show significant influence on the process objective functions or that can be fixed at an optimum value independently of other factors. In addition to the CO_2 absorber decision variables enumerated above, other two groups of process decision variables have been found to affect the optimal performance of the capture process. Namely, these are the **CO_2 desorber decision variables**, which highly influence the energetic performance of the capture process but hardly affect the productivity of the process, i.e.:

- Pressure, $P_{CO_2 des}$ [Pa].
- Cold-rich bypass split fraction, f_{cr} [–].

and the **FG-WW section decision variables**, which have a minor effect on the energy performance and productivity of the capture process but are still important to meet process specifications and constraints, i.e.:

- Temperature of the washing water or solvent-lean aqueous solution, T^{FG-WW}_{lean} [°C].
- Liquid-to-gas flowrate ratio, $(L/G)^{FG-WW}$ [kg kg^{-1}], at the top of the washing column.
- Apparent solvent concentration, $\hat{c}^{FG-WW}_{solvent}$ [$mol_{solvent}$ $kg^{-1}_{H_2O}$] of the washing water or solvent-lean aqueous solution.
- Pumparound split fraction, f^{FG-WW}_{s} [–], recycled to the washing column.
- Pumparound temperature, T^{FG-WW}_{pa} [°C].

Step 2. Multi-objective heuristic optimization that allows to identify the values of the **decision variables** that optimize the performance of the capture process applied to the new case, i.e. the CO_2 absorber decision variables, the CO_2 desorber decision variables and the FG-WW section decision variables enumerated above. As for the **objective functions** used in the heuristic optimization, these are the CO_2 capture efficiency, the productivity, and the specific equivalent work. Let us better identify them.

The **CO_2 capture efficiency**, ψ [–], is the ratio between the CO_2 flowrate sent to storage and the CO_2 flowrate entering the capture process within the flue gas. When avoiding CO_2 losses in the capture process, and neglecting the very minor amount of CO_2 captured in the NH_3 absorber, the overall CO_2 capture efficiency corresponds to the CO_2 capture efficiency in the CO_2 absorber:

$$\psi = \frac{\dot{m}^{FG,in}_{CO_2} - \dot{m}^{FG,out}_{CO_2}}{\dot{m}^{FG,in}_{CO_2}} \tag{25}$$

where $\dot{m}^{FG,in}_{CO_2}$ and $\dot{m}^{FG,out}_{CO_2}$ are the CO_2 mass flowrate contained in the flue gas entering and exiting the CO_2 absorber [kg_{CO_2} s^{-1}], respectively.

The **productivity**, Pr [$kg_{CO_2 captured}$ m^{-3} h^{-1}], provides an estimation of the total volume of the absorption columns and it is an indication of the trends of capital costs of the capture process. The CO_2 absorber cost has been reported to be the main component of the CAPEX, with a contribution ranging from 30% for solvents with fast CO_2 absorption rates to 60% for solvents that require a taller CO_2 absorption column (Tsay et al., 2019). We can expect that the operating conditions of the CO_2 absorber will have to be adapted to cope with the different flue gas composition, affecting significantly the design of the column. Therefore, here we consider the size of

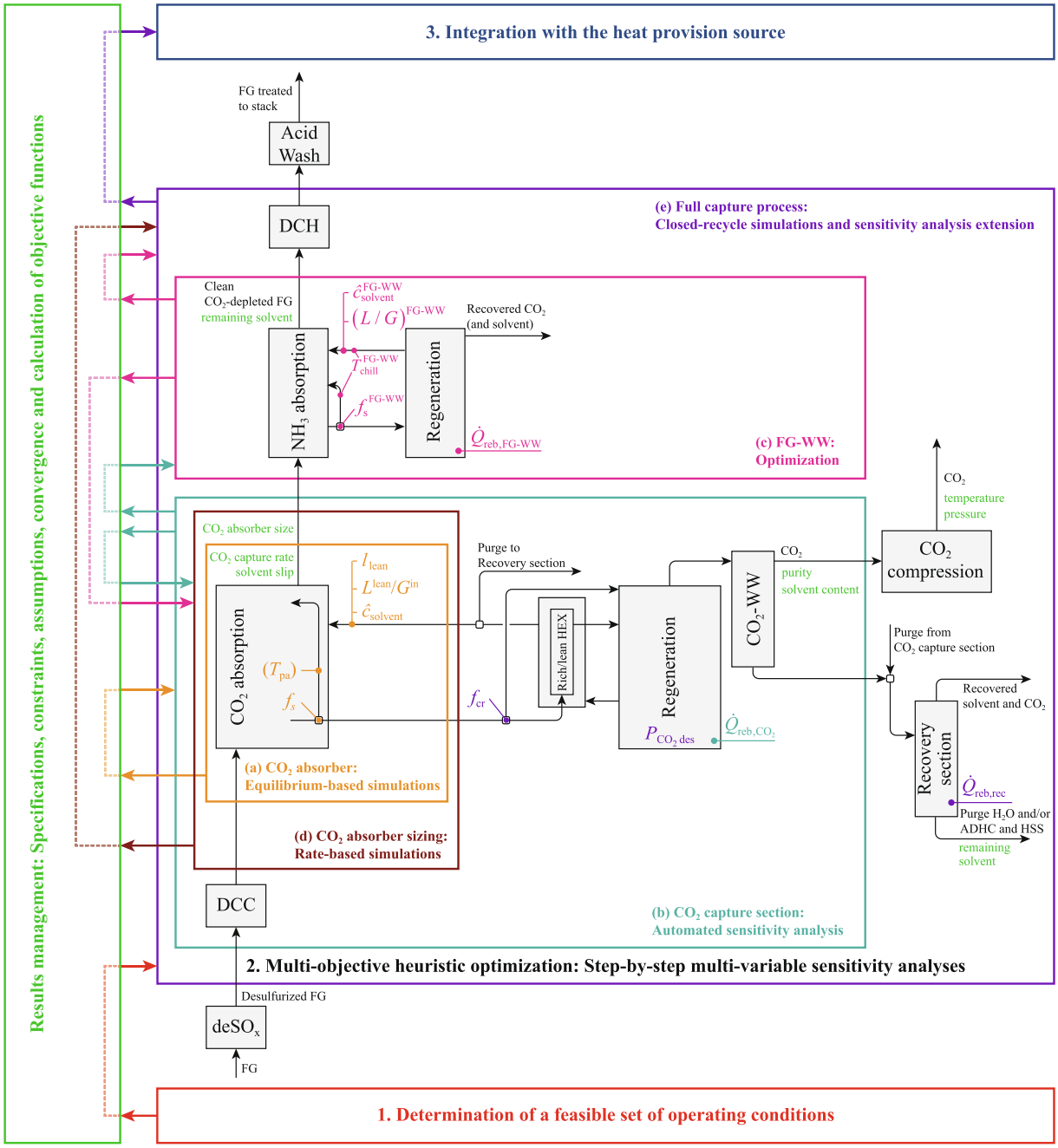

Fig. 3. Schematic of the sequential process optimization strategy proposed for the optimization of a solvent-based capture process when applied to a new flue gas composition and/or to a new CO_2 capture efficiency specification.

the CO_2 absorber as driver in the determination of the different process productivities:

$$\mathrm{Pr} = \frac{\dot{m}_{CO_2}^{FG,in} - \dot{m}_{CO_2}^{FG,out}}{V_{CO_2 abs}} \tag{26}$$

where $V_{CO_2 abs}$ is the volume of packing required in the CO_2 absorber if: (i) cylindrical shape is considered, and (ii) a hydraulic load at the bottom of the column at 70% of flooding is defined (van der Spek et al., 2019).

The **specific equivalent work**, ω [MJ $kg_{CO_2 captured}^{-1}$], is considered as indicator of the energy demand of the CO_2 capture process. Consequently, the energy requirements of all key consumers have to be converted to specific equivalent work.

- The thermal energy required in each reboiler and supplied by steam is converted to equivalent work, $\omega_{reb,i}$, applying the Carnot cycle, as follows:

$$\omega_{reb,i} = \frac{\dot{Q}_{reb,i}}{\dot{m}_{CO_2}^{FG,in} - \dot{m}_{CO_2}^{FG,out}} \left(1 - \frac{T_{amb}}{T_{reb,i} + \Delta T_{steam}}\right) \tag{27}$$

where i refers to the CO_2 desorber ("CO_2"), the desorber of the FG-WW section ("FG-WW") and the solvent reclaimer in the recovery section ("rec") (see Fig. 1), $\dot{Q}_{reb,i}$ [MW_{th}] is the thermal duty required in each reboiler, $T_{reb,i}$ [K] is the reboiler temperature, ΔT_{steam} [K] is the temperature difference, above the reboiler operating temperature, of the steam that provides heat, and T_{amb} [K] is the temperature of the environment.

- The chilling duty (i.e. below ambient temperature), which is required for the pumparound stream of each absorber, i.e. CO_2 absorber and NH_3 absorber, is converted to equivalent work, $\omega_{chill,i}$, as:

$$\omega_{chill,i} = \frac{\dot{Q}_{chill,i}/COP_i}{\dot{m}_{CO_2}^{FG,in} - \dot{m}_{CO_2}^{FG,out}} \quad (28)$$

where i refers to the chillers specified in Fig. 1, $\dot{Q}_{chill,i}$ [MW_{th}] is the chilling duty of chiller i, and COP_i is the coefficient of performance (Anantharaman et al., 2017).

- Auxiliaries, such as fans and pumps, require electric energy. The equivalent work associated with the cooling water pumps was computed from the cooling demand, $\dot{Q}_{cool}$ [MW_{th}], and a conversion factor, ϕ_{cool} [MW_{el} MW_{th}^{-1}], typical of forced draft cooling towers.

$$\omega_{aux} = \frac{\frac{\dot{W}_{fan}^{ideal}}{\eta_{comp}} + \frac{1}{\eta_{pump}}\sum_i \dot{W}_{pump,i}^{ideal} + \phi_{cool}\sum_j \dot{Q}_{cool,j}}{\dot{m}_{CO_2}^{FG,in} - \dot{m}_{CO_2}^{FG,out}} \quad (29)$$

where i and j, here, refers to the pumps and coolers specified in Fig. 1, respectively, and η_{pump} and η_{comp} are the efficiency of pumps and compressors (and fan), respectively.

- The CO_2 compression, $\omega_{CO_2 comp}$, is calculated from detailed Aspen Plus simulations using the compressor configuration provided by Manzolini et al. (2011).

In practice, such multi-objective heuristic optimization consists of successive multi-variable sensitivity analyses that start with the stand-alone CO_2 absorber and that, step-by-step, add units and process sections to the simulations to finalize with the optimization of the full capture process. Whenever possible, this optimization can be carried out via a full mathematical optimization, which should reduce the computing time, while likely leading to very similar optimal performance. These sub-steps are referred to as *Step 2(a)* to *Step 2(e)* in Fig. 3, where the boxes contain the unit operations and sections simulated in each sub-step, which can be identified with the process flow diagram shown in Fig. 1. More specifically, the sub-steps of Step 2 consist of the following actions:

Step 2(a).
Equilibrium-based simulations of the CO_2 absorber, whereby the CO_2 absorber decision variables are screened through an extensive, automated sensitivity analysis (via direct Aspen Plus-Matlab connection). Simulations are equilibrium-based and use calibrated Murphree efficiencies obtained in Step 1 for the feasible set of operating conditions of the new case. Due to the low computational time required for each equilibrium-based simulation of the CO_2 absorber, i.e. 1 to 2 s per simulation, the goal of this first screening is to find those sets of operating conditions that lead to successful simulations of the CO_2 absorber in terms of convergence and fulfilment of the process specifications and constraints.

Step 2(b).
Automated sensitivity analysis of the CO_2 capture section, where the operating conditions that lead to successful simulations of the CO_2 absorber are used to run the whole CO_2 capture section. In order to maximize the number of converged simulations and minimize the required computational time, still accounting for the main energy consumers of the capture process, the simulation is limited to the process boundaries drawn in Fig. 3. Namely, the simulation of the FG-WW section and the recovery section is avoided since including the associated recycle streams would lead to more than a twofold increase of the simulation time. The absolute reboiler duty of the CO_2 desorber, $\dot{Q}_{reb,CO_2}$, is included in the sensitivity analysis. In practice, there exists only one value of $\dot{Q}_{reb,CO_2}$ for each set of operating conditions of the CO_2 absorber that is able to meet the CO_2 loading specified in the CO_2-lean stream while not leading to excess CO_2 stripping. The flowrate of the purge stream is calculated to avoid the accumulation of water within the CO_2 capture section and/or of ADHC and HSS, depending on the specific solvent and process configuration. The solvent content targeted in the CO_2-lean stream is met by a make-up stream of aqueous solvent. It is also worth noting that the pinch point temperature in the rich/lean heat exchanger can be reached internally, instead of between inlet and outlet streams, when partial evaporation is obtained at the desorber inlet (optimal condition). Finally, although the CO_2 desorber decision variables affect considerably the performance of the main energy consumer of the capture process, i.e. the reboiler of the CO_2 desorber, they have a minor effect on the optimal set of operating conditions of the CO_2 absorber. Therefore, $P_{CO_2 des}$ and f_{cr} are fixed at this stage at values that do not hinder the convergence of the process simulation and that allow for the fulfilment of the process specifications and constraints.

Step 2(c)
Optimization of the FG-WW section. Here, the successful simulations of the CO_2 capture section provide data for the FG-WW section. A rigorous optimization based on successive quadratic programming (SQP) is carried out, allowed by the lower complexity and lower NH_3 and CO_2 concentration in the flue gas with respect to the CO_2 capture section. In particular, the specific reboiler duty of the desorber can be minimized by tuning the FG-WW decision variables and the absolute reboiler duty of the desorber, $\dot{Q}_{reb,FG-WW}$.

Step 2(d)
Rate-based simulations of the CO_2 absorber, for the most promising sets of operating conditions of the column found so far in terms of energy demand of the capture process. Rate-based simulations of the CO_2 absorber are performed, finding the size of the packing that meets the CO_2 capture efficiency and solvent loss for the corresponding equilibrium-based simulations at the same set of operating conditions of the CO_2 absorber. Those sets of operating conditions for which the rate-based simulation is not able to meet the equilibrium-based simulation results are considered as infeasible absorber designs thus discarded for further process optimization.

Step 2(d)
Full capture process simulations, whereby those sets of operating conditions showing the most promising results in terms of energy performance and productivity are considered for a further multivariable sensitivity analysis in which the operating variables of the CO_2 desorber are varied. Here, full capture process simulations are performed, including the recovery section and the CO_2 compression section, whose performance is influenced drastically by the operating variables of the CO_2 desorber.

Step 3. Integration with the heat provision source, where the results of Step 2 are used for integration with the CO_2 point source of the new case, therefore considering how energy is supplied to the CO_2 capture process. The specific equivalent work is related to the total equivalent electrical work required by the capture plant if the capture process is applied to a power plant; the energy demand of the capture plant leads to a decrease of the specific electrical output of the power plant due to: (i) the electricity demand

required in the auxiliaries, CO_2 compressor and chillers of the capture process, and (ii) the steam required in the reboilers of the capture plant, which is withdrawn from the power plant instead of being used to produce electricity. Nevertheless, capture processes applied to industrial CO_2 points sources are not necessarily built integrated with or next to a power plant, hence there might not be steam available for solvent regeneration, and electricity should be imported from the grid. If the capture process is to be integrated with a specific, defined, CO_2 point source, the SPECCA (Specific Primary Energy Consumption per CO_2 Avoided) index is preferred instead to assess its energy performance. Specifically, for the application of the CAP to cement plants for CO_2 capture, the SPECCA, ζ [$MJ_{LHV}/kg_{CO_2\,avoided}$], is defined as (Voldsund et al., 2019):

$$\zeta = \frac{(q_{clk})_{CCS} - (q_{clk})_{ref}}{(e_{clk})_{ref} - (e_{clk})_{CCS}} \quad (30)$$

where q_{clk} is the specific primary energy consumption of the cement plant per unit of mass of clinker produced, considering the low heating value (LHV) of the fuel consumed, [MJ_{LHV}/t_{clk}]; and e_{clk} is the specific CO_2 emissions of the cement plant per unit of mass of clinker produced [kg_{CO_2}/t_{clk}]. The subscripts "ref" and "CCS" refer to the reference cement plant without CO_2 capture and to the cement plant with CO_2 capture, respectively. Two significantly different scenarios have been considered for the production of the steam demanded by the capture process (Anantharaman et al., 2017): (i) steam is produced in a natural gas (NG) boiler built specifically on-site to supply steam, and only steam, for the CAP; or, (ii) steam is imported from an external coal-fired combined heat and power (CHP) plant located in the neighbourhood of the cement plant.

Assumptions regarding the climate impact and energy conversion efficiencies associated with each steam production scenario and with electricity imported from the grid are given in Table 4, along with additional assumptions required for process simulation and for the computation of the objective functions. The parameters required for energy calculations, along with the flue gas and CO_2 exiting conditions, have been retrieved from literature (Voldsund et al., 2019; Anantharaman et al., 2017). For the sake of simplicity, impurities in the flue gas have not been considered in this case study. The columns in the flue gas pre-conditioning section and in the flue gas heating section have been simulated as a DCC and as a DCH, respectively, without considering the acidic compounds contained in the inlet flue gas and the NH_3 leaving the top of the NH_3 absorber. The required flowrates of fresh make-up aqueous NH_3 (or caustic) solution and aqueous H_2SO_4, as well as the flowrate of pure solid $(NH_4)_2SO_4$ can be computed from simple straightforward mass balances.

Table 4
Basic set of assumptions considered for the process simulation and optimization.

CO_2 stream for transport by pipeline to storage	
Temperature [°C]	28
Pressure [bar]	110
Composition	
CO_2 concentration [vol%]	> 95
H_2O concentration [ppm_{wt}]	< 200
NH_3 concentration [ppm_v]	< 50
CO_2-depleted flue gas at the stack	
Temperature [°C]	> 40
NH_3 concentration [ppm_v]	< 10
Purge liquid streams	
NH_3 concentration [ppm_{wt}]	< 150
Flue gas pre-conditioning section	
SO_2 concentration entering the CO_2 absorber [ppm]	0
Make-up streams	
Temperature [°C]	20
Apparent NH_3 content in make-up NH_3 streams [mass frac.]	0.25
Auxiliaries, utilities and environment	
Ambient temperature (T_{amb}) [°C]	15
Cooling water temperature [°C]	18.2
Pinch point temperature for heat exchangers [°C]	
Liquid–liquid (ΔT_{L-L})	3
Evaporator of chilling utility (ΔT_{evap})	5
Reboiler (ΔT_{steam})	10
Pump efficiency (η_{pump}) [–]	0.76
Fan and compressor efficiency (η_{comp}) [–]	0.81
Cooling water system power demand (ϕ_{cool}) [MW_{el}/MW_{th}]	0.02
COP = $f(T_{chill})$ [–] (see Table 6.15 in Anantharaman et al. (2017))	5.5–10.2
Electricity generation efficiency [%]	45.9
Electricity generation specific CO_2 emissions [kg/MWh]	262
Steam from NG boiler	
Boiler efficiency (LHV basis) [%]	90
Specific CO_2 emissions [kg/GJ_{th}]	56.1
Steam from coal-fired CHP plant	
(see Table 6.1 in Anantharaman et al. (2017) for $T_{steam} = 100 - 160$°C)	
Efficiency for coal to power w/o steam extraction [MW_{el}/MW_{th}]	0.391
Efficiency for steam to power = $f(T_{steam})$ [MW_{el}/MW_{th}]	0.133–0.266
Specific CO_2 emissions = $f(T_{steam})$ [kg/MWh_{th}]	116–231

5. Results and discussion

In this section, the results of applying the sequential process simulation and optimization strategy described in Section 4 to the case study are presented and discussed.

5.1. Step 1 – Determination of a feasible set of operating conditions

Firstly, the initial set of operating conditions of the CO_2 absorber of the CAP were obtained for increasing CO_2 concentration in the flue gas (Cement Case 18 and Cement Case 22 in Table 1). As starting point, we used the set of operating conditions of the CO_2 absorber calculated by Sutter et al. (2016), which was obtained aiming at minimizing the energy consumption of the capture process when applied to coal-fired power plants, i.e. Power Case in Table 1, for the same process specifications and constraints of this case study (see Table 2). Starting from these values, we have manually adapted the operating conditions to the cement flue gas characteristics, thus identifying a preliminary set of parameters (named "init" in Table 5) and their associated range (named "min" and "max" in Table 5).

Secondly, the Murphree efficiency values, which result from the rate-based simulation of the CO_2 absorber operating with the initial set of decision variables, are computed for each CO_2 concentration in the inlet flue gas. Murphree efficiency values depend on the number of equilibrium stages considered for the equilibrium-based simulation of the absorption column. In this case study, Murphree efficiencies for CO_2 and NH_3 have been obtained for an equilibrium-based model that considers 5 equilibrium stages in the NH_3-slip reduction section and 15 equilibrium stages in the CO_2-uptake section of the CO_2 absorber, as in the column implemented by Sutter et al. (2016) for the power plant application. The Murphree efficiency values obtained in this case study range from 0.07 to 0.2 for CO_2 and from 0.7 to 0.9 for NH_3. The full set of values for every equilibrium stage is reported in the Supplementary Material, for each flue gas composition. The temperature and gas composition profiles obtained with equilibrium- and rate-based simulations are compared in the Supplementary Material for the initial set of operating conditions. Remarkably, they lead to similar results for both cement flue gas compositions.

Thirdly, the range of operating conditions selected for the CO_2 absorber decision variables are obtained as a result of the first full

Table 5
Operating conditions of the CO_2 absorber considered in the sequential simulation and heuristic optimization of the CAP applied to cement plants for CO_2 capture. For each cement flue gas composition it is indicated: (i) the initial set of operating conditions for each cement case resulting from the preliminary adaptation of the CAP developed for the power plant application to the new flue gas conditions; and, (ii) the range of input variables that has been tested, identified by "min" and "max". Moreover, the table also shows the optimal set of operating conditions found by Sutter et al. (2016) (Power Case).

Param.	Units	Power Case $y_{CO_2}^{FG,in} = 0.14$	Cement Case 18 $y_{CO_2}^{FG,in} = 0.18$				Cement Case 22 $y_{CO_2}^{FG,in} = 0.22$			
		best (Sutter et al., 2016) P	**init**	**min**	**max**	**best** C.18	**init**	**min**	**max**	**best** C.22
$\hat{c}_{NH_3}$	$[mol_{NH_3}\ kg_{H_2O}^{-1}]$	8.9	8.0	4.0	10.0	7.0	8.0	4.0	10.0	5.0
l_{lean}	$[mol_{CO_2}\ mol_{NH_3}^{-1}]$	0.352	0.331	0.25	0.45	0.350	0.331	0.25	0.45	0.362
L^{lean}/G^{in}	$[kg\ kg^{-1}]$	4.2	4.9	3.5	8.5	5.0	6.0	4.0	10.0	7.0
f_s	[–]	0.28	0.25	0.05	0.45	0.25	0.18	0.05	0.45	0.15
T_{pa}	[°C]	10	5	5	19	12	5	5	19	13

process equilibrium-based simulations and subsequent single variable sensitivity analyses. These values are given in Table 5. As planned in our overall methodology, the CO_2 desorber decision variables, i.e. $P_{CO_2 des}$ and f_{cr}, are fixed at 10 bar and 0.08, respectively, in Step 2(b) and varied between 5 and 27.5 bar and between 0.02 and 0.16, respectively, in Step 2(e). In addition, conditions and design specifications fixed for the remaining sections of the CAP are provided in Table 6, whose values are either extracted from the power plant application (Sutter et al., 2016), or the result of the aforementioned single variable sensitivity analyses. The latter variables are highlighted in Table 6.

5.2. Step 2 – Multi-objective heuristic optimization

Making use of the ranges of the input parameters selected in the previous step, 36,252 and 31,752 different sets of CO_2 absorber operating conditions were considered in **Step 2(a)** -CO_2 absorber as standalone equipment- for Cement Case 18 and Cement Case 22, respectively. Among these, 4,617 and 3,421 equilibrium-based simulations of the CO_2 absorber converged within the specifications and were therefore retained for further analysis, first in the CO_2 capture section simulation (**Step 2(b)**), and then in the FG-WW section simulation (**Step 2(c)**). As a result, 3,125 and 1,665 simulations, each characterized by a different set of operating conditions of the CO_2 absorber, reached convergence within specifications and constraints for each cement case. Finally, rate-based simulations of the CO_2 absorber were run in **Step 2(d)**, out of which 2,384 and 1,263 for Cement Case 18 and Cement Case 22, respectively, led to a feasible result, i.e. there exists a CO_2 absorber design that is able to meet the CO_2 capture efficiency and the NH_3 loss obtained by the corresponding equilibrium-based simulation.

Fig. 4 shows the results obtained for the optimization of the CAP after Step 2(d) of the sequential simulation and optimization strategy, applied to Cement Case 18; each symbol corresponds to a different set of operating conditions of the CO_2 absorber, which has produced a converged simulation within specifications. Fig. 4(a) shows the results in the specific equivalent work-CO_2 capture efficiency plane. Specific equivalent work minimization and CO_2 capture efficiency maximization are opposing objectives, defining a frontier where the CO_2 capture efficiency can only be increased at the cost of a higher minimum specific equivalent work (and vice versa), the so-called "pareto front". The use of new, calibrated Murphree efficiency values for each new case in the equilibrium-based simulations provided a good approximation of the mass transfer limitations computed by the rate-based model. As a consequence, infeasible absorber designs providing higher efficiency at constant energy requirement than the pareto front points, defined exclusively by feasible design operating conditions, are only obtained at very high capture efficiency. Fig. 4(b) shows the results in the ω^*-Pr plane for a narrow range of CO_2 capture efficiencies around the targeted value for this case study, i.e. 0.9. For constant ψ, the specific equivalent work minimization and productivity maximization are also opposing objectives: the increase in productivity can only be achieved by increasing the minimum specific equivalent work, thus forming a pareto front. Similar plots to those shown in Fig. 4 have been generated for Cement Case 22. The resulting

Table 6
Operating and design conditions fixed in all simulations of the CAP independently of the flue gas specifications, organized by process section. Unless specified, pressure drop in columns is neglected. In addition, the temperature of make-up streams entering the capture process, i.e. water and chemicals, is assumed to be 20°C in all cases.

CO_2 capture section	
Pressure at the top/bottom of the CO_2 absorber [bar]	1.01/1.04
CO_2 absorber packing	25-mm Pall rings
CO_2-lean stream inlet temperature to CO_2 absorber [°C]	21.2
Pressure drop in the CO_2 desorber [bar]	0.5
Number of equilibrium stages in the CO_2 desorber	10
Feed stage of the hot CO_2-rich stream to the CO_2 desorber	7
FG-WW section	
Purity NH_3-lean solution ($\hat{c}_{NH_3}^{FG-WW}$) $[mol_{NH_3}\ kg_{H_2O}^{-1}]$	0.05
Pressure at the top of the NH_3 absorber [bar]	1.01
Number of equilibrium stages in the NH_3 absorber	50
Murphree efficiency for CO_2 ($E_{CO_2}^M$) in the NH_3 absorber	0.015
Pumparound stage entering the NH_3 absorber	15
Temperature of chilled streams ($T_{lean}^{FG-WW} = T_{pa}^{FG-WW} = T_{chill}^{FG-WW}$) [°C]	1.5
Temperature of condenser NH_3 desorber [°C]	68
Pressure at the top of the NH_3 desorber [bar]	1.01
Number of equilibrium stages in the NH_3 desorber	9
Feed stage to the NH_3 desorber	4
Flue gas pre-conditioning section	
Number of equilibrium stages in the DCC	5
Pressure at the top of the DCC [bar]	1.01
Temperature of water entering the top of the DCC [°C]	21.2
Liquid-to-gas flowrate ratio [kg/kg]	2
Fan inlet/outlet pressure [bar]	1.01/1.1
Flue gas heating section	
Number of stages in the DCH	5
Pressure at the top of the DCH [bar]	1.01
CO_2-WW section	
Number of equilibrium stages in the CO_2-WW column	4
Temperature of water entering the CO_2-WW column [°C]	50
Liquid-to-gas flowrate ratio [kg/kg]	0.3
CO_2 recovery section	
Number of equilibrium stages in the appendix stripper	4
Pressure at the top of the appendix stripper [bar]	1.15
CO_2 compression section	
Number of inter-cooled compression stages	3

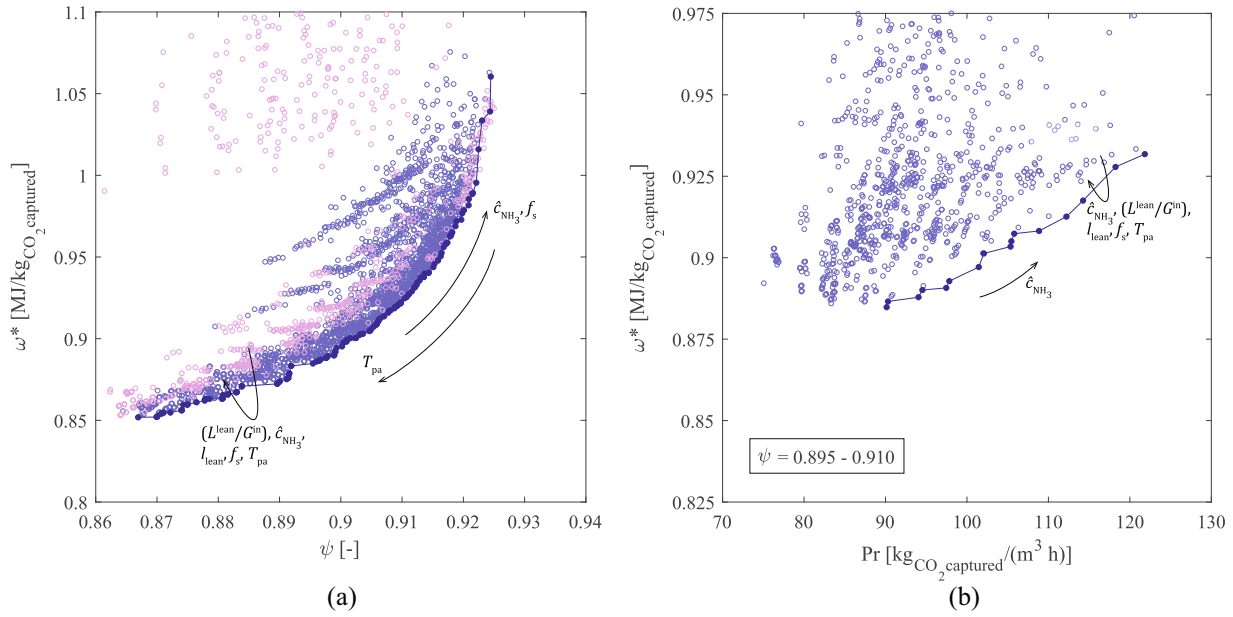

Fig. 4. Specific equivalent work vs.: (a) CO_2 capture efficiency values; and, (b) productivity at CO_2 capture efficiency between 0.895 and 0.910, of all simulations converged and fulfilling specifications and constraints for Cement Case 18 after Step 2(d) of the sequential heursitic optimization strategy (○). Note that the specific equivalent work, ω^*, considered at this point: (i) does not include the energy consumers from the recovery and CO_2 compression sections, and (ii) is normalized by the CO_2 mass flowrate in the stream sent to CO_2 compression. On the contrary, the CO_2 capture efficiency, ψ, is computed as that of the CO_2 absorber, which is the expected value when including the recovery section and recycle stream to the CO_2 absorber. The pareto front is defined by the assemble of linked points (●) at the frontier of the cloud of points. Lighter symbols in (a) (○) account for those sets of operating conditions of the CO_2 absorber that did not lead to feasible column designs resulting from the rate-based simulations performed in Step 2(d), and are therefore not shown in (b) and discarded for further process optimization. The black arrows indicate the qualitative trends of the decision variables towards and along the pareto front.

pareto fronts, which provide the optimum set of operating conditions for the CO_2 absorber in each cement case, are shown in Fig. 5, along with the results of the optimized CAP applied to the power plant case calculated by Sutter et al. (2016). For given CO_2 capture efficiency and productivity values, the minimum specific equivalent work decreases when increasing the CO_2 concentration in the inlet flue gas, which is in line with the trend of the minimum separation energy as a function of the CO_2 partial pressure in the inlet flue gas. Although the effect of the CO_2 absorber decision variables on the performance of the CAP are subject to complex interdependencies, qualitative trends with respect to the optimal conditions can be observed (see black arrows in Fig. 4 and Fig. 5):

- We can move towards higher CO_2 capture efficiency while minimizing the energy cost by simultaneously increasing $\hat{c}_{NH_3}$ and f_s and decreasing T_{pa}, with a negligible variation of L^{lean}/G^{in} and l_{lean}.
- The productivity can be increased while keeping constant the CO_2 capture efficiency and minimizing the specific equivalent work of the process by increasing $\hat{c}_{NH_3}$. The increase in $\hat{c}_{NH_3}$ is compensated by a slight increase in l_{lean} for Cement Case 18 and by a slight decrease in L^{lean}/G^{in} for Cement Case 22.
- If the CO_2 concentration in the inlet flue gas increases, and the CO_2 capture efficiency and the productivity have to be kept constant, the specific energy consumption is minimized by simultaneously increasing L^{lean}/G^{in} and T_{pa} and decreasing $\hat{c}_{NH_3}$ and f_s.

The optimum values for each CO_2 absorber decision variable along the pareto fronts shown in Fig. 5 are provided in the Supplementary Material.

As far as the optimization of the FG-WW section is concerned, in all points belonging to the pareto fronts the optimal values of the flowrate of the NH_3-lean stream and the NH_3 absorber pumparound split fraction are 0.1 [kg kg^{-1}] and very close to 0, respectively. The NH_3 concentration and temperature of the NH_3-lean stream, and the temperature of the pumparound were fixed at the values provided in Table 6.

The points C.18 and C.22 in Fig. 5(b), which correspond to the minimum specific equivalent work for each CO_2 concentration in the inlet flue gas, have been selected for further comparison with the process developed and optimized for the power plant case (Sutter et al., 2016), i.e. point P in Fig. 5. It can be noted that the set of operating conditions that minimizes ω^* for both C.18 and C.22 leads to similar productivity values among them and with respect to the operating conditions P of the power plant case. The operating conditions of the CO_2 absorber corresponding to C.18 and C.22 are shown in Table 5, labelled as "best".

Furthermore, Fig. 6 shows the liquid composition profiles along the CO_2 absorber for the operating conditions P, C.18 and C.22; the liquid apparent composition is plotted in the ternary phase diagram (TPD) of the CO_2-NH_3-H_2O system, in which each symbol is color-coded to indicate the corresponding temperature. For a detailed explanation of the TPD applied to the CO_2-NH_3-H_2O system, the reader is referred to the work of Sutter et al. (2015). Firstly, for all cases, the liquid compositions along the CO_2 absorber have similar CO_2 loadings, i.e. the composition of the pumparound stream entering the top of the CO_2 absorber is next to the solubility curve, but outside the S-L equilibrium region. As pointed out by Sutter et al. (2015), the pumparound of the CO_2 absorber is one of the critical points regarding solid formation, and the process optimization is constrained to avoid the formation of solids in this stream. In addition, Fig. 6 illustrates that the apparent concentration of NH_3 in the solvent at the optimum set of operating conditions of the CO_2 absorber decreases when increasing the CO_2 concentration in the inlet flue gas, as mentioned above. As a consequence, the driving force for CO_2 transfer from the vapour to the liquid phase is kept approximately constant when increasing the

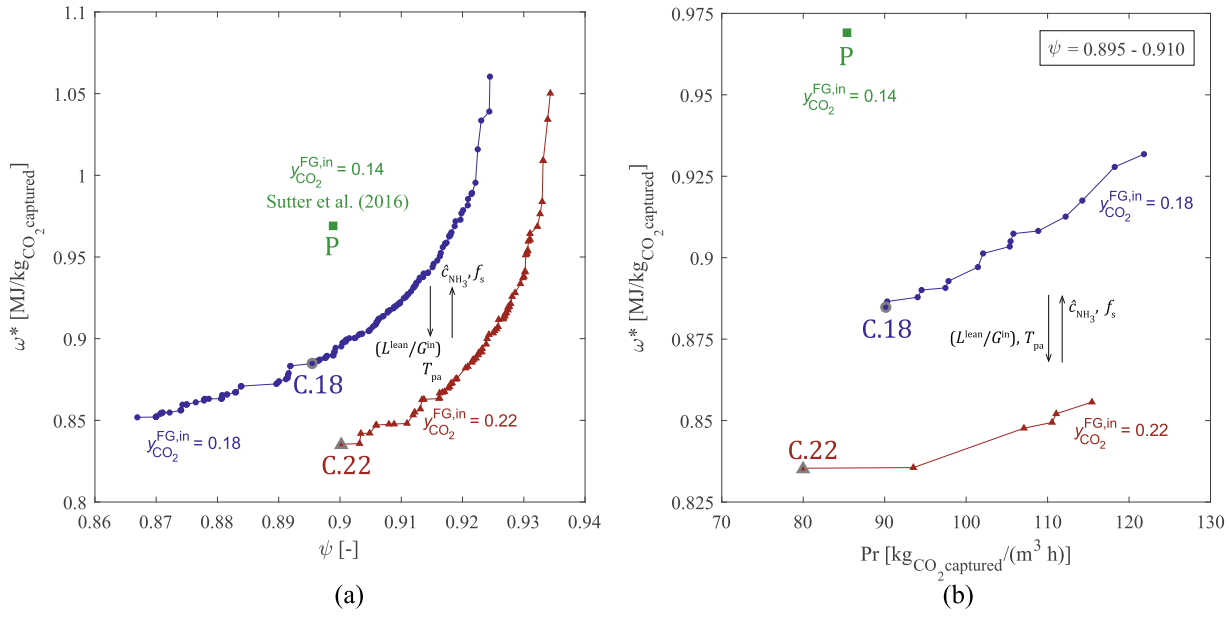

Fig. 5. Resulting pareto fronts of the optimization of the CO_2 absorber operating conditions of the CAP for cement application in the plane: (a) specific equivalent work vs. CO_2 capture efficiency; and, (b) specific equivalent work vs. productivity at fixed CO_2 capture efficiency between 0.895 and 0.910. In addition to the pareto fronts obtained for Cement Case 18 (●) and for Cement Case 22 (▲), the results of the optimized CAP applied to the power plant case found by Sutter et al. (2016) is also represented (■) as reference and labelled as P. The performance of the CO_2 absorber operating variables for Cement Case 18 and Cement Case 22 selected for further analysis and comparison are labelled as C.18 and C.22, respectively. In this figure, ω^* and ψ are computed as specified in the caption of Fig. 4. The black arrows indicate the qualitative trends of the decision variables to move between pareto fronts obtained for different CO_2 concentration in the inlet flue gas.

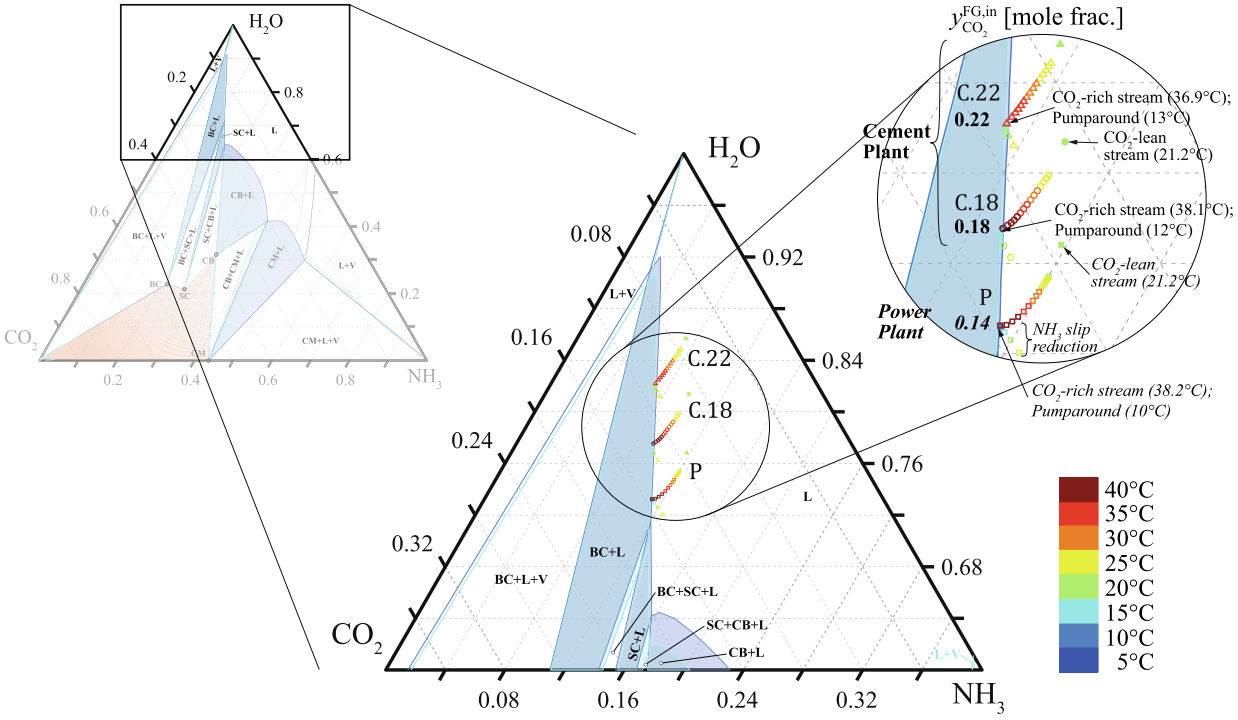

Fig. 6. Profile of the liquid phase along the CO_2 absorber for the optimal set of operating conditions of the CO_2 absorber that minimizes the energy consumption for Cement Case 18 (circles) and Cement Case 22 (triangles), and for the Power Case (squares). Temperatures along the column can be read using the color code (rounded to 5°C). For the sake of visuality, each symbol corresponds to the apparent composition of a stage of the equilibrium-based simulation with Murphree efficiencies. The phase diagram considers apparent weight fraction of CO_2, NH_3 and H_2O and applies to 1.013 bar and 10 and 15°C, i.e. the closest temperatures rounded to 5 °C steps of the pumparound stream resulting from each case. The phase regions are labelled as V for vapour, L for liquid and S for solid.

CO_2 concentration in the flue gas by decreasing the NH_3 concentration in the solvent; then, the solvent CO_2 uptake capacity is maintained by increasing the CO_2-lean liquid-to-gas flowrate ratio. Not surprisingly, the liquid composition profiles along the CO_2 absorber have similar features as in the power plant profile: (i) efficient capture of CO_2 along the whole CO_2 uptake section, (ii) drastic removal

of NH_3 in the NH_3 slip removal section, (iii) and continuous increase of temperature from the top of the column with a maximum value close to the bottom of the column. The corresponding gas composition and temperature profiles resulting from the rate-based simulations are provided in the Supplementary Material: the equilibrium-based model is able to reproduce accurately the profiles obtained using the rate-based model, thus confirming the validity of the simplifications introduced in Step 2 of this optimization procedure.

The heuristic optimization was extended in **Step 2(e)** to the CO_2 desorber decision variables and their effect on the specific equivalent work for the low energy CO_2 absorber operating conditions, i.e. C.18, C.22 and P in Table 5. The variables $P_{CO_2 des}$ and f_{cr} highly influence the energetic performance not only of the CO_2 desorber, but also of the recovery section and of the CO_2 compression section. These effects are illustrated in Fig. 7 for Cement Case 18 using the operating conditions defined by C.18. More specifically, Figs. 7 (a)–(c) show the effect of the CO_2 desorber pressure and the cold-rich bypass split fraction on the energy requirements of the CO_2 desorber, Figs. 7(d)–(f) show their effect on the performance of the recovery section, and Figs. 7(g)–(i) on the energy requirements associated with CO_2 compression. As expected, the CO_2 desorber reboiler duty, $\dot{Q}_{reb,CO_2}$, can be decreased by increasing $P_{CO_2 des}$, as shown in Fig. 7(a). There exists an optimum f_{cr} value for each $P_{CO_2 des}$ that maximizes the heat exchanged in the rich/lean heat exchanger, thus eventually minimizing $\dot{Q}_{reb,CO_2}$; the optimal f_{cr} decreases when increasing $P_{CO_2 des}$. On the other hand, the CO_2 desorber reboiler temperature increases with increasing pressure. As a result, the specific equivalent work associated with the steam required in the reboiler of the CO_2 desorber finds its minimum along the whole range of pressures considered in this study, for a narrow range of cold-rich split fraction values that vary with the pressure level. However, not only must the CO_2 desorber strip-off CO_2 from the CO_2-rich solvent, but also provide a CO_2 vapour stream with enough purity for transportation and storage. Specifically, NH_3 is vaporized together with CO_2 in the CO_2 desorber due to its high volatility, and has to be removed from the vapour phase and re-condensed in the upper part of the column: The goal is to limit the concentration of NH_3 in the CO_2 gas stream so as to avoid solid formation downstream in the process. This is achieved by means of the cold-rich bypass. Therefore, the values of $P_{CO_2 des}$ and f_{cr} that minimize $\dot{Q}_{reb,CO_2}$ are found in the operating area closest to solid formation: If the cold-rich bypass split fraction is too low, solids may form in the condensate of the CO_2 stream generated before or during compression as a result of an excessive NH_3 content in the gas stream leaving the CO_2-WW section.

As far as the reboiler duty of the appendix stripper in the recovery section, $\dot{Q}_{reb,rec}$, is concerned, it increases: (i) when decreasing f_{cr} for a fixed $P_{CO_2 des}$, and (ii) for lower $P_{CO_2 des}$ at constant f_{cr}, as shown in Fig. 7(d). In both cases, the NH_3 mole fraction in the CO_2 stream leaving the CO_2 desorber, $y_{NH_3}^{CO_2-WW,in}$, increases as a consequence of a higher temperature and of a lower pressure, respectively, as shown in Fig. 7(f). Therefore, the fresh water make-up (and associated purge stream) required in the CO_2-WW section, $F_{H_2O}^{CO_2-WW,in}$, to remove NH_3 from the CO_2 stream increases (Fig. 7 (e)), thus increasing the appendix stripper reboiler duty required to recuperate the NH_3 (and CO_2) contained in the purged streams.

Finally, the pressure at the CO_2 desorber has opposing effects on the CO_2 compression and on the CO_2-rich stream pumping to the CO_2 desorber, as shown in Fig. 7(g) and Fig. 7(h), respectively; as a result, the sum of the two energy contributors, i.e. $\omega_{CO_2 comp} + \omega_{aux}$, decreases when increasing $P_{CO_2 des}$ for the range of operating conditions studied in this case study, as shown in Fig. 7(i).

Overall, there exists a combination of values of $P_{CO_2 des}$ and f_{cr} that minimizes the total specific equivalent work of the capture process for each CO_2 concentration in the inlet flue gas; this is shown as ω isoregions in Fig. 8(a). In addition to the infeasible region due to solid formation, Fig. 8(a) also includes the regions of the CO_2 desorber decision variables that are infeasible as they would not meet constraints regarding maximum temperature of the solvent, T_{reb,CO_2}, and maximum NH_3 concentration in the CO_2 stream entering the CO_2 compression section, $y_{NH_3}^{CO_2 comp,in}$ (whose values are reported in Table 2). The optimal CO_2 desorber pressure and cold-rich bypass split fraction values decrease when increasing the CO_2 concentration in the flue gas, i.e. P, C.18 and C.22 in Table 5, leading to optimal $P_{CO_2 des}$ and f_{cr} of 25.0 bar and 0.05, of 22.5 bar and 0.0475 and of 17.5 bar and 0.045, respectively. As a result, the total specific equivalent work can be decreased when increasing the CO_2 concentration in the inlet flue gas, from 1.12 MJ $kg_{CO_2 captured}^{-1}$ for the optimal Power Case, P, to 1.04 and 0.98 MJ $kg_{CO_2 captured}^{-1}$ for C.18 and C.22, respectively. Notably, the optimal set of CO_2 desorber decision variables and the feasible region of operating conditions for each inlet flue gas composition are a consequence of the corresponding optimal set of operating conditions of the CO_2 absorber. For example, the optimal apparent NH_3 concentration in the solvent decreases when increasing the CO_2 concentration in the inlet flue gas; thus the maximum CO_2 desorber pressure is limited to lower values by the reboiler temperature constraint.

Furthermore, Fig. 8(b) provides the specific equivalent work break-down for the optimal operating conditions in terms of minimal energy consumption for each flue gas composition. All contributions, except for that associated with the CO_2 compression, decrease when increasing the CO_2 concentration. In addition and not surprisingly, in all cases the main contribution to the overall specific equivalent work required for the CAP stems from the steam required in the CO_2 desorber for solvent regeneration. Consequently, the optimization of the operating conditions of the capture process is driven by the decrease of the reboiler duty of the CO_2 desorber. In this work, the CAP reboiler duty for the CO_2 desorber ranges between 2.1 and 2.2 MJ_{th} $kg_{CO_2 captured}^{-1}$ when varying the CO_2 mole fraction in the inlet flue gas from 0.14 to 0.22. This compares closely with the thermal energy requirements of the best performing amine solvents (Leeson et al., 2017; Rochelle et al., 2019).

5.3. Step 3 – Integration with the heat provision source

The integration with the heat provision source is carried out and guided by the computation of the SPECCA of the capture process, ζ, considering features and CO_2 emissions of the electricity and steam consumed. The SPECCA is of paramount importance as it provides a fair comparison with alternative capture technologies, which might require different steam quality or might not need steam at all. This is even more important for industrial processes where steam and waste heat might or might not be available (e.g., integrated steelworks vs. cement).

When recomputing the optimization results obtained after Step 2(d), i.e. excluding $P_{CO_2 des}$ and f_{cr}, to identify the pareto front consisting of the minimum SPECCA values, we recognize that:

- If steam is produced in a NG boiler, the SPECCA is minimized by decreasing the reboiler duty of the CO_2 desorber. Accordingly, this requires to decrease $\hat{c}_{NH_3}$, l_{lean} and L^{lean}/G^{in} with respect to the optimal operating conditions obtained when minimizing the specific equivalent work.

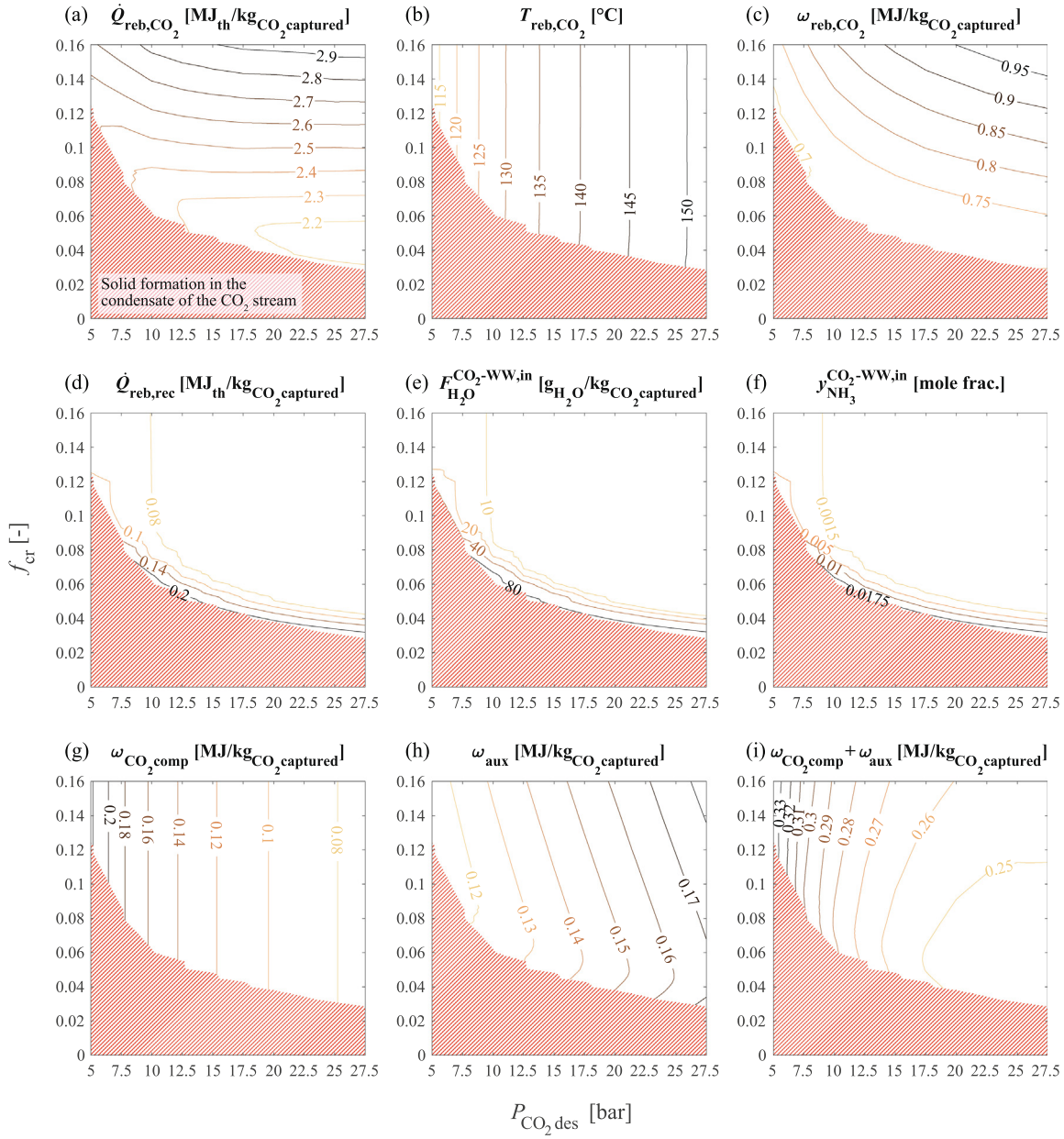

Fig. 7. Response surfaces obtained in the plane cold-rich bypass split fraction vs. CO_2 desorber pressure applied to the optimal set of operating conditions defined by C.18 in Table 5 obtained for Cement Case 18, for the following variables: (a) heat duty required at the reboiler of the CO_2 desorber; (b) temperature at the reboiler of the CO_2 desorber; (c) specific equivalent work associated with the thermal energy required in the reboiler of the CO_2 desorber; (d) heat duty required by the reboiler of the recovery section; (e) fresh water make-up flowrate required in the CO_2-WW section; (f) NH_3 mole fraction in the CO_2 stream leaving the top of the CO_2 desorber; (g) specific equivalent work associated with the CO_2 compression section; (h) specific equivalent work related to the auxiliary units of the CO_2 capture process; and (i) sum of the two latter specific equivalent work variables. The striped area represents the infeasible region of the process, where solids may form in the condensate of the CO_2 stream before or during CO_2 compression.

- If steam is produced in a CHP plant, it is important to account for both flow rate and temperature of the imported steam. Therefore, the SPECCA is minimized by increasing $\hat{c}_{NH_3}$, l_{lean} and L^{lean}/G^{in} with respect to the optimal operating conditions obtained when minimizing the specific equivalent work.

In both cases, we can vary the capture efficiency (or the productivity) by playing with the remaining CO_2 absorber operating conditions. The optimal set of operating conditions of the CO_2 absorber decision variables for Cement Case 18 depending on the energy performance indicator are provided in the Supplementary Material.

However, we note that the pareto front identified by minimizing the specific equivalent work (see Fig. 5) is very close to the pareto identified by minimizing the SPECCA when reporting both in the SPECCA-efficiency (or SPECCA-productivity) plane. Or, in other words, the SPECCA values calculated with the optimal operating conditions identified by the specific equivalent work minimization either belong or are very close to the pareto front obtained when directly minimizing the SPECCA. This is illustrated in greater detail in Fig. 9. Figs. 9(a) and 9(b) report the results for the NG boiler case, in the SPECCA-efficiency and SPECCA-productivity planes, respectively. Figs. 9(c) and 9(d) report the results for the CHP plant case, again in the SPECCA-efficiency and SPECCA-productivity planes, respectively. It can be noted, that the coloured area (blue for

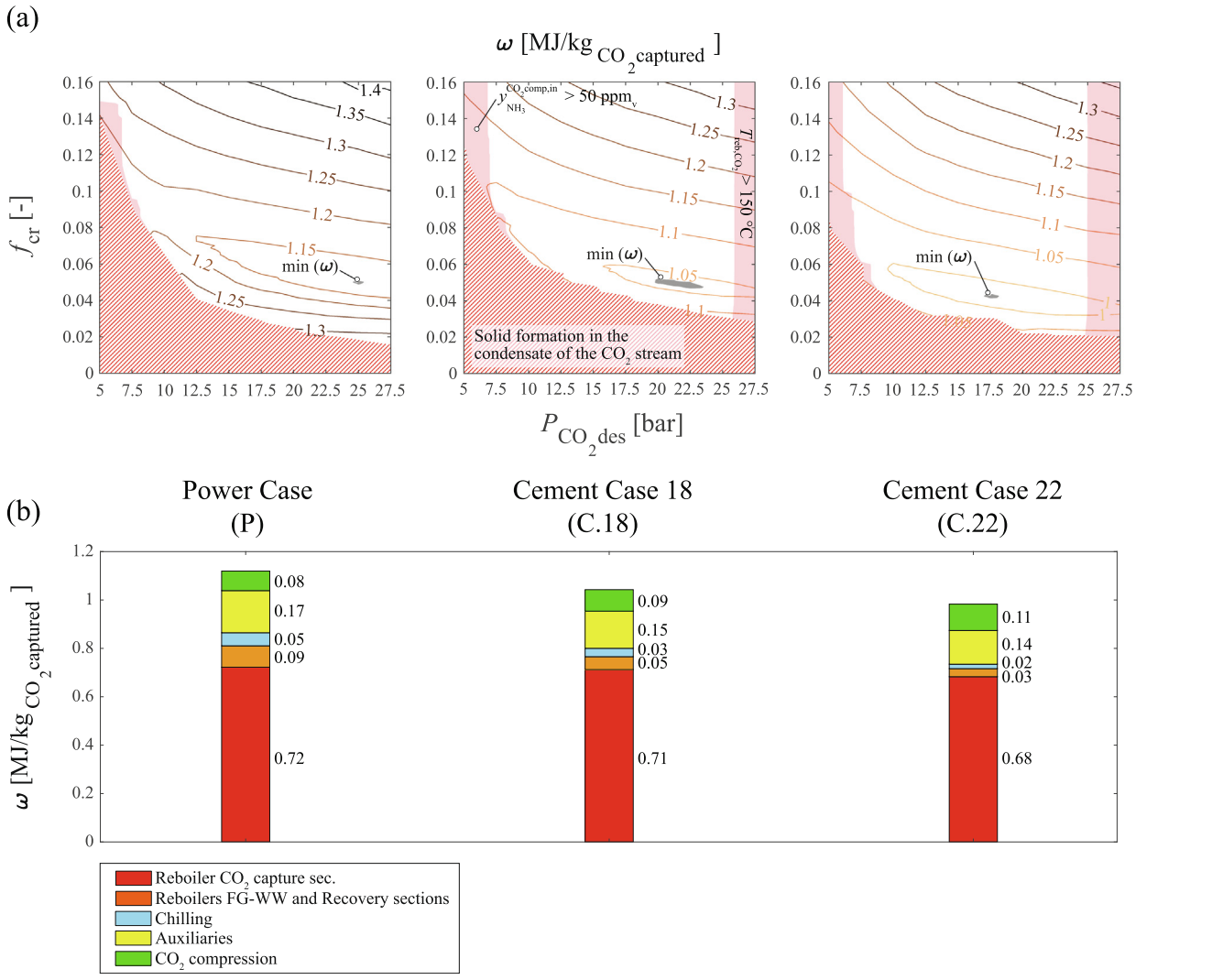

Fig. 8. (a) Response surfaces obtained in the plane cold-rich bypass split fraction vs. CO_2 desorber pressure for the overall specific equivalent work of the CAP using the optimal sets of operating conditions of the CO_2 absorber defined, from left to right, by P, C.18 and C.22 in Table 5; the infeasible region of the process is given by the striped area, where solids may form, and by the red shadowed regions, which define the range of CO_2 desorber operating conditions at which the NH_3 concentration in the CO_2 stream sent to compression, at the left, and the CO_2 desober reboiler temperature, at the right, would not meet the process constraints. (b) Contributions of the key energy consumers to the minimum overall specific equivalent work of the CAP applied to different inlet flue gas compositions; operating conditions correspond to those defined by P, C.18 and C.22 in Table 5, from left to right, for the CO_2 absorber, and to those leading to the minimum ω in (a) for the CO_2 desorber.

Cement Case 18 and red for Cement Case 22), which is obtained considering the pareto points obtained by minimizing the specific equivalent work, lead to SPECCA values which are less than 3% greater than the minimum SPECCA value achievable for a given productivity of the process. This translates in a mere average difference of 0.1 and 0.05 $MJ_{LHV}\ kg^{-1}_{CO_2 avoided}$ for the NG boiler case and for the CHP plant case, respectively.

When recomputing the optimization results obtained after Step 2(e), i.e. including the CO_2 desorber operating conditions, to minimize the SPECCA, the optimal values of $P_{CO_2 des}$ and f_{cr} depend on the heat provision source and differ from those obtained when minimizing the specific equivalent work. The effect of $P_{CO_2 des}$ and f_{cr} on the SPECCA is shown in Fig. 10 for Cement Case 18 (at the set of operating conditions of the absorber that minimizes the specific equivalent work, i.e. defined by C.18 in Table 5). We recognize that:

- If steam is produced in a NG boiler, the SPECCA is minimized by increasing $P_{CO_2 des}$, since this minimizes the reboiler duty of the CO_2 desorber. However, the upper bound is limited by the reboiler temperature; f_{cr} also strongly affects the SPECCA and has to be adjusted to an optimal value that decreases with increasing $P_{CO_2 des}$.
- If steam is produced in a CHP plant, $P_{CO_2 des}$ has opposing effects on flow rate and temperature of the imported steam. Although the SPECCA is minimized by decreasing $P_{CO_2 des}$, the SPECCA is close to its minimum regardless of $P_{CO_2 des}$; as for the NG boiler case, f_{cr} has to be adjusted to an optimal value that also decreases with increasing $P_{CO_2 des}$.

Nevertheless, it can be similarly noted here, that the grey-coloured area which is obtained considering the CO_2 desorber operating conditions that minimize the specific equivalent work, lead to SPECCA values that are less than 3% greater than the minimum SPECCA value. This translates in a mere difference of less than 0.1 $MJ_{LHV}\ kg^{-1}_{CO_2 avoided}$.

Overall, the energetic optimization of the capture process considering the real steam source, i.e. using a set of operating conditions of the CO_2 absorber and of the CO_2 desorber that minimizes the SPECCA, improves the energy performance of the process

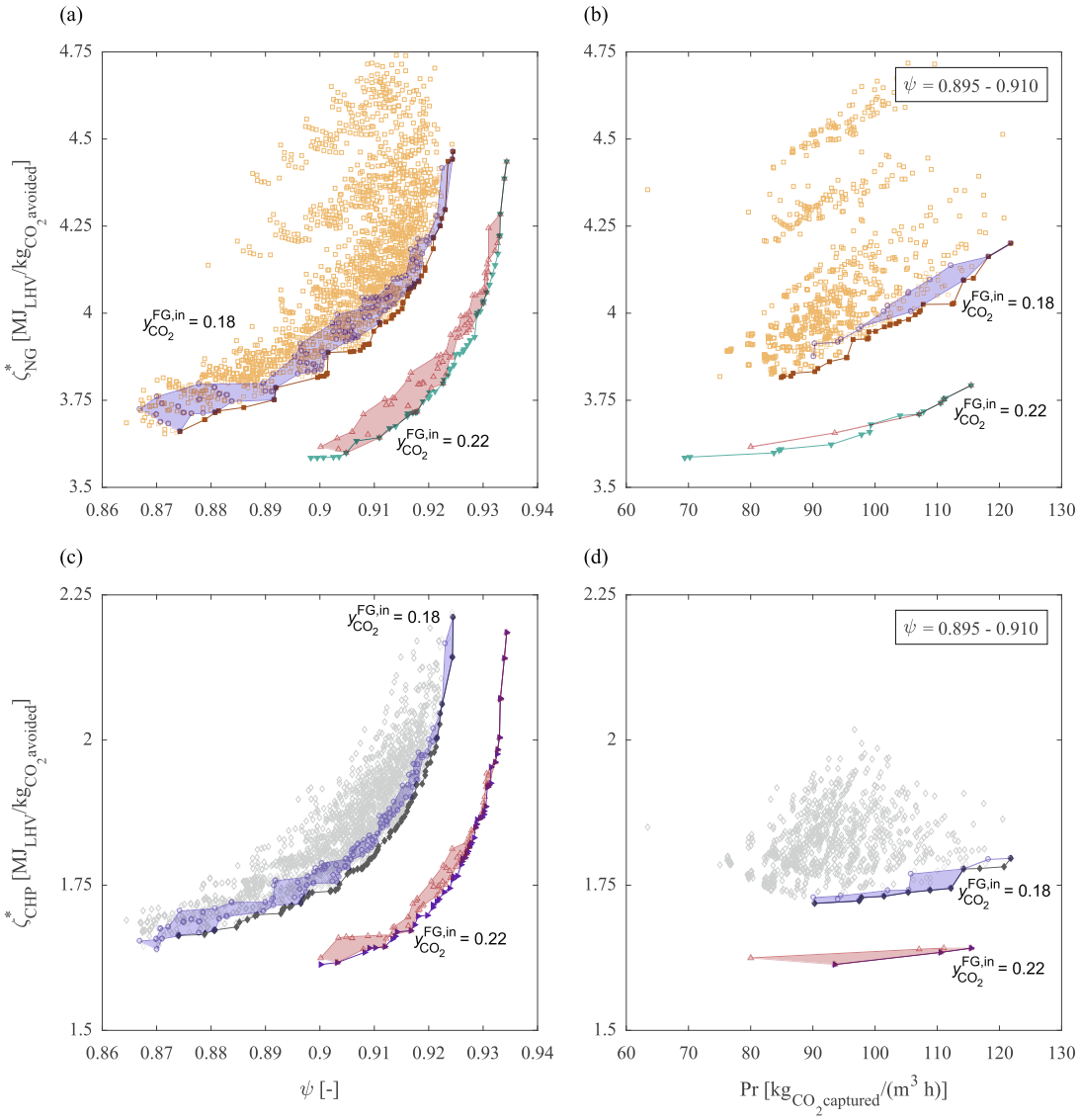

Fig. 9. Pareto fronts of the optimization of the CO_2 absorber operating conditions in the plane: (a) SPECCA-CO_2 capture efficiency for steam produced in a NG boiler; (b) SPECCA-productivity for steam produced in a NG boiler and CO_2 capture efficiency between 0.895 and 0.910; (c) SPECCA-CO_2 capture efficiency for steam imported from a CHP plant; and, (d) SPECCA-productivity for steam imported from a CHP plant and CO_2 capture efficiency between 0.895 and 0.910. Pareto fronts are shown for Cement Case 18 using a NG boiler (■) or a CHP plant (◆) as steam source, and for Cement Case 22 using a NG boiler (▼) or a CHP plant (►) as steam source. The results of all simulations converged and fulfilling specifications and constraints after Step 2(d) are also shown for both steam production types, i.e. NG boiler (□) and CHP plant (◇), for Cement Case 18. The points belonging to the pareto fronts obtained in Fig. 5 when minimizing the specific equivalent work are shown for Cement Case 18 (○) and Cement Case 22 (△); the regions defined by these points have been shadowed to show their performance with respect to the paretos obtained when minimizing the SPECCA. ζ^* and ψ are computed following the description included in the caption of Fig. 4.

by less than 6% with respect to considering the specific equivalent work. Therefore, the capture process can be optimized using the specific equivalent work, ω, as energy performance indicator, while neglecting the effect of the steam source on the process optimization. On the other hand, including the SPECCA index is of paramount importance to understand the best steam supply option: when steam can be imported from a CHP plant, the CAP's SPECCA is as low as 2.5 MJ_{LHV} $kg^{-1}_{CO_2\,avoided}$ for Cement Case 18. This translates into a SPECCA reduction of 35% with respect to producing steam in a NG boiler built on-site.

6. Conclusions

Solvent-based post-combustion CO_2 capture technologies have been investigated extensively for their application to power plants. Such capture processes include a rather large number of unit operations that need complex simulation tools for their description, including accurate description of thermodynamics, reaction kinetics, and transport phenomena, particularly mass transfer. Therefore, the optimization of such complex processes from a scientific perspective is very cumbersome and time consuming, leading to very long development times. Regarding the model, experimental tests at pilot plant scale are usually performed for model validation purposes. As far as the process optimization is concerned, recycle of streams among different process sections, along with the necessity of rate-based simulations for equipment sizing increase considerably simulation times and worsen convergence, thus hindering the optimization of the process.

To overcome these difficulties, we have developed a new methodology that uses the available know-how in the literature to optimize the full process flow diagram of solvent-based capture

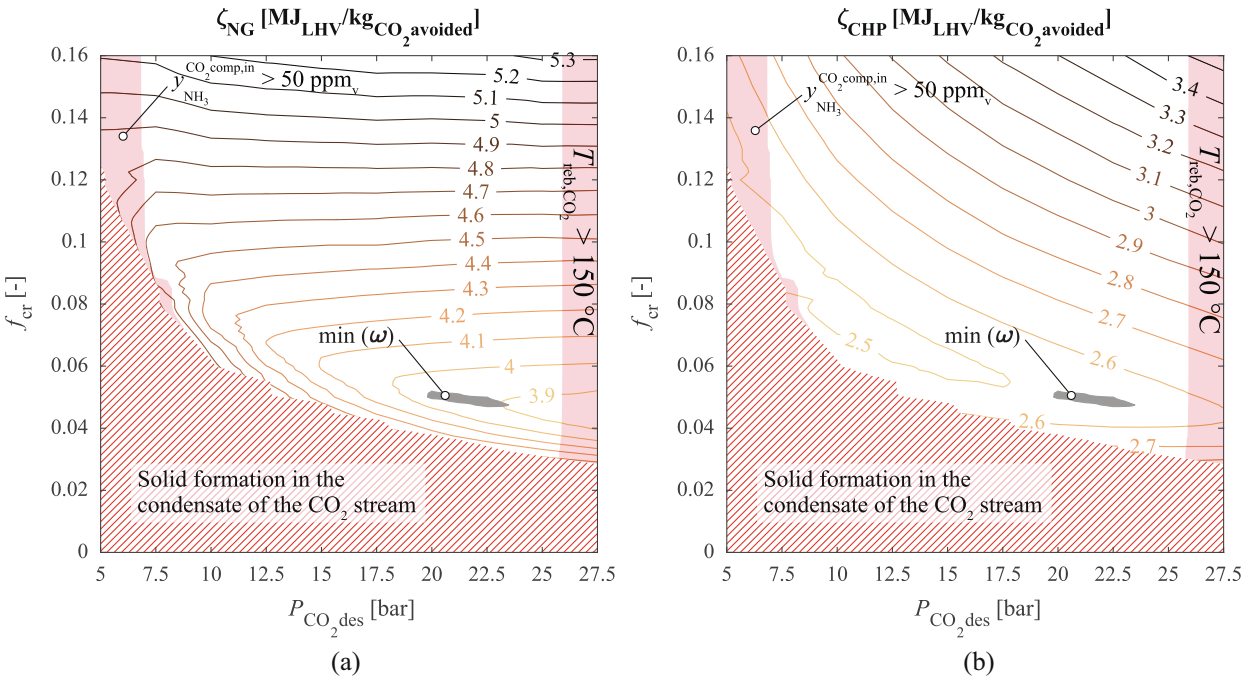

Fig. 10. Isoregions obtained in the plane cold-rich bypass split fraction vs. CO_2 desorber pressure for the overall SPECCA when: (a) steam is produced in a NG boiler; and, (b) steam is imported from a CHP plant. The grey-coloured area identifies the region for minimum specific equivalent work. All simulations have been performed at the set of operating conditions of the CO_2 absorber defined by C.18 in Table 5 for Cement Case 18.

processes that are to be applied to a new flue gas composition and/or for a different process specification, e.g. for a new CO_2 capture efficiency, but reducing the time for development from years to months.

Firstly, our methodology consists of a procedure that provides comprehensive criteria based on physico-chemical properties of the system for the selection and/or calibration of the thermodynamic model, transport property models, kinetic models and model numerical options that compose the rate-based model. As a result, a model that can be used reliably in a broad range of operating conditions for process optimization is obtained from experimental data available in literature, thus avoiding new experimental tests, and minimizing at the same time the simulation effort required for model development and validation. The main guidelines proposed for model development and calibration, whose validity has been proven with the case study presented in this work, are the following:

- The selection of the thermodynamic model should not only be based on its accuracy in predicting the VLE experimental data, but should also be guided by the capacity of the model in reproducing the experimental evidence regarding solid formation. Avoiding solid formation is one of the constraints of the process optimization, so that its accurate prediction is of paramount importance to obtain realistic results.
- If liquid-phase reaction kinetics obtained for the range of operating conditions explored in the process optimization are not available in literature, we propose to use instead kinetic models obtained at infinite dilution. Then, the model is extrapolated to the concentration range considered in the optimization problem by means of activity-based kinetics, whose kinetic constants are computed from the corresponding kinetic constants reported in literature and obtained at infinite dilution.
- Density and transport property models should consider not only solvent measurements, but also data corresponding to CO_2-loaded solutions when available in the literature.
- Geometric discretization of the liquid film with half of the discretization segments within the chemical film thickness is proposed. Considering these pre-requisites, the number of discretization segments and the value of the discretization ratio is determined from the value of the Hatta number, thus avoiding time consuming trial-and-error approaches.

Secondly, we propose a procedure for process optimization that applies a number of strategies and approximations aiming at decreasing the required time without compromising the validity of the results. These strategies and approximations, whose validity has also been proven by means of the case study included in this work, are the following:

- The step-wise simulation and optimization approach allows to limit the number of simulations of the full capture process only to those sets of operating conditions that converge and meet specifications and constraints for the different process sections. We have shown that the decision variables of the CO_2 absorber, of the FG-WW section and of the CO_2 desorber can be optimized step by step.
- Rate-based simulations are avoided for full capture process simulations and are only performed for the stand-alone CO_2 absorber at conditions that meet the specifications and constraints of the full capture process.
- Mass transfer limitations in the CO_2 absorber are successfully accounted for by means of new, calibrated Murphree efficiency values implemented in the equilibrium-based simulations for each new optimization case, which lead to feasible CO_2 absorber designs for a majority of operating conditions.
- A single set of Murphree efficiency values can be used for the optimization of the process for given CO_2 concentration in the flue gas and specification of CO_2 capture efficiency. This set is computed from the rate-based simulation of the CO_2 absorber operating with the initial conditions.

- In order to determine a feasible set of operating conditions that can be used as initial condition for the optimization of the process, a reference design of the same or similar capture technology is used as point of departure, using the know-how about the process to reach the (new) CO_2 capture efficiency for the new flue gas composition.
- While the comparison with respect to other types of technologies requires the integration of the solvent-based capture process with the steam provision source, in this work we have shown that the process optimization itself can be carried out considering the specific equivalent work as energy consumption indicator. This makes the optimization methodology more general and independent of the boundary conditions of the CO_2 industrial point source as far as the steam generation is concerned.

As far as the specific results obtained for the case study are concerned, the optimal CAP operation when increasing the CO_2 concentration in the flue gas, for constant CO_2 capture efficiency, requires the decrease of the apparent NH_3 concentration in the solvent and of the solvent temperature in the CO_2 absorber, and the increase of the liquid-to-gas flowrate ratio in the CO_2 absorber. In addition, the CO_2 loading in the CO_2-lean stream is adapted in all cases in such a way that the pumparound stream is pushed towards the solubility limit at optimal operating conditions. As a consequence of the lower apparent NH_3 concentration in the solvent, the optimal pressure at the CO_2 desorber decreases for increasing CO_2 concentration in the inlet flue gas. As a result of the optimization of the process, the energy consumption is decreased for increasing CO_2 concentration in the inlet flue gas, thus leading to reboiler duties as low as 2.1 $MJ_{th}\ kg^{-1}_{CO_2 captured}$ for the CAP applied to cement plants, while maintaining the productivity of the CO_2 absorber, thus the column height, in values in the order of those typical of the power plant application.

Besides being applied to new point sources with different CO_2 concentration in the flue gas, as in the case study presented in this work, and targeting different specifications of CO_2 capture efficiency and CO_2 purity, this methodology can also be applied to find the new optimal set of operating conditions of the capture process when the CO_2 concentration in the inlet flue gas varies over time because of changes in the fuel/raw meal inlet composition, or because of greater flowrate of air slipping into the industrial manufacturing process. In the context of the case study of this work and of the latter application, the optimization results obtained using the methodology presented in this work have been used by Voldsund et al. (2019) and by Gardarsdottir et al. (2019) for the techno-economic assessment of the CAP, in comparison with other capture technologies when applied to cement plants for CO_2 capture.

CRediT authorship contribution statement

José-Francisco Pérez-Calvo: Conceptualization, Methodology, Software, Validation, Formal analysis, Writing - original draft, Writing - review & editing, Visualization. **Daniel Sutter:** Conceptualization, Methodology, Writing - review & editing. **Matteo Gazzani:** Conceptualization, Methodology, Software, Writing - review & editing, Visualization. **Marco Mazzotti:** Conceptualization, Writing - review & editing, Supervision, Project administration, Funding acquisition.

Declaration of Competing Interest

The authors declare that they have no known competing financial interests or personal relationships that could have appeared to influence the work reported in this paper.

Acknowledgements

This project has been partially funded through the European Union's Horizon 2020 research and innovation programme under grant agreement No. 641185. This work was partially supported by the Swiss State Secretariat for Education, Research and Innovation (SERI) under contract number 15.0160.

The authors would like to thank Kaj Thomsen (Department of Chemical and Biochemical Engineering, Technical University of Denmark) for making the thermodynamic model available, and for providing the relevant software.

Appendix A. Supplementary material

Supplementary data associated with this article can be found, in the online version, at https://doi.org/10.1016/j.cesx.2020.100074.

References

Abanades, C., Cinti, G., Berstad, D., Hoenig, V., Hornberger, M., Jordal, K., Al, E., 2019. CEMCAP Strategic conclusions – progressing CO2 capture from cement towards demonstration. CEMCAP Deliverable D2.11., Tech. rep. (feb 2019). doi:10.5281/zenodo.2593135. https://doi.org/10.5281/zenodo.2593135#.Xc6UuK6RvVp.mendeley

Abu-Zahra, M.R.M., Abbas, Z., Singh, P., Feron, P., 2013. Carbon dioxide post-combustion capture: solvent technologies overview, status and future directions. Mater. Processes Energy: Commun. Curr. Res. Technol. Dev., 923–934

Abu-Zahra, M.R., El Nasr, A.S., Al Hajaj, A., Goetheer, E.L., 2016. Techno-economics of liquid absorbent-based post-combustion CO 2 processes. In: Absorption-Based Post-Combustion Capture of Carbon Dioxide, Elsevier Inc., Ch. 27, pp. 685–710. doi:10.1016/B978-0-08-100514-9.00027-5.

Amirkhosrow, M., Pérez-Calvo, J.-F., Gazzani, M., Mazzotti, M., Nemati Lay, E., 2020. Rigorous rate-based model for CO2 capture via monoethanolamine-based solutions: effect of kinetic models, mass transfer, and holdup correlations on prediction accuracy. Sep. Sci. Technol., 1–19 https://doi.org/10.1080/01496395.2020.1784943.

Anantharaman, R., Berstad, D., Cinti, G., De Lena, E., Gatti, M., Gazzani, M., Hoppe, H., Martinez, I., Monteiro, J.G.M.-S., Romano, M., Roussanaly, S., Schols, E., Spinelli, M., Storset, S., van Os, P., Voldsund, M., 2017. D3.2 CEMCAP framework for comparative techno-economic analysis of CO2 capture from cement plants, Tech. rep.. doi:10.1111/j.1552-6909.2009.01070.x. https://doi.org/10.5281/zenodo.1257112#.XcVkX2NGuBm.mendeley https://www.sintef.no/globalassets/sintef-energi/cemcap/d3.2-cemcap-framework-for-comparative-techno-economic-analysis-of-co2-capture-from-cement-plants_.pdf.

Anderson, C., Harkin, T., Ho, M., Mumford, K., Qader, A., Stevens, G., Hooper, B., 2013. Developments in the CO2CRC UNO MK 3 process: a multi-component solvent process for large scale CO2 capture. In: Energy Procedia, vol. 37, Elsevier, pp. 225–232. doi:10.1016/j.egypro.2013.05.106. https://www.sciencedirect.com/science/article/pii/S1876610213001161.

Anderson, C., Hooper, B., Qader, A., Harkin, T., Smith, K., Mumford, K., Pandit, J., Ho, M., Lee, A., Nicholas, N., Indrawana, I., Gouw, J., Xiao, J., Thanumurthy, N., Temple, N., Stevens, G., Wiley, D., 2014. Recent developments in the UNO MK 3 Process – a low cost, environmentally benign precipitating process for CO2 capture. In: Energy Procedia, vol. 63, Elsevier, pp. 1773–1780. doi:10.1016/j.egypro.2014.11.184. https://www.sciencedirect.com/science/article/pii/S1876610214019997.

Andersson, V., Franck, P.Å., Berntsson, T., 2016. Techno-economic analysis of excess heat driven post-combustion CCS at an oil refinery. Int. J. Greenhouse Gas Control 45, 130–138. https://doi.org/10.1016/j.ijggc.2015.12.019. https://www.sciencedirect.com/science/article/pii/S1750583615301626.

Arasto, A., Tsupari, E., Kärki, J., Pisilä, E., Sorsamäki, L., 2013. Post-combustion capture of CO2 at an integrated steel mill – Part I: Technical concept analysis. Int. J. Greenhouse Gas Control 16, 271–277. https://doi.org/10.1016/j.ijggc.2012.08.018. https://www.sciencedirect.com/science/article/pii/S1750583612002150.

Aspen Technology Inc., 2014. Aspen Plus help file.

Asprion, N., 2006. Nonequilibrium rate-based simulation of reactive systems: simulation model, heat transfer, and influence of film discretization. Ind. Eng. Chem. Res. 45 (6), 2054–2069. https://doi.org/10.1021/ie050608m.

Astarita, G., 1967. Mass Transfer with Chemical Reaction. Elsevier. https://books.google.ch/books?id=UKxTAAAAMAAJ.

Augustsson, O., Baburao, B., Dube, S., Bedell, S., Strunz, P., Balfe, M., Stallmann, O., 2017. Chilled ammonia process scale-up and lessons learned. In: Energy Procedia, vol. 114, Elsevier, pp. 5593–5615. doi:10.1016/j.egypro.2017.03.1699. https://www.sciencedirect.com/science/article/pii/S1876610217319008.

Barker, D.J., Turner, S.A., Napier-Moore, P.A., Clark, M., Davison, J.E., 2009. CO2 capture in the cement industry. In: Energy Procedia, vol. 1, Elsevier, pp. 87–94.

doi:10.1016/j.egypro.2009.01.014. https://www.sciencedirect.com/science/article/pii/S1876610209000150.
Bjerge, L.M., Brevik, P., 2014. CO2 capture in the cement industry, norcem CO2 capture project (Norway). Energy Procedia, vol. 63. Elsevier Ltd, pp. 6455–6463. https://doi.org/10.1016/j.egypro.2014.11.680.
Bollinger, R., Muraskin, D., Hammond, M., Kozak, F., Spitznogle, G., Cage, M., Varner, M., Sherrick, B., Varner, M., 2010. CCS project with Alstom's chilled ammonia process at AEP's mountaineer plant. In: Air and Waste Management Association – 8th Power Plant Air Pollutant Control Mega Symposium 2010, vol. 1, pp. 539–586.
Boot-Handford, M.E., Abanades, J.C., Anthony, E.J., Blunt, M.J., Brandani, S., Mac Dowell, N., Fernández, J.R., Ferrari, M.C., Gross, R., Hallett, J.P., Haszeldine, R.S., Heptonstall, P., Lyngfelt, A., Makuch, Z., Mangano, E., Porter, R.T., Pourkashanian, M., Rochelle, G.T., Shah, N., Yao, J.G., Fennell, P.S., 2014. Carbon capture and storage update. doi:10.1039/c3ee42350f. http://xlink.rsc.org/?DOI=C3EE42350F.
Boundary Dam Carbon Capture Project, 2020. https://www.saskpower.com/our-power-future/infrastructure-projects/carbon-capture-and-storage/boundary-dam-carbon-capture-project http://saskpowerccs.com/ccs-projects/boundary-dam-carbon-capture-project/.
Brúder, P., Grimstvedt, A., Mejdell, T., Svendsen, H.F., 2011. CO2 capture into aqueous solutions of piperazine activated 2-amino-2-methyl-1-propanol. Chem. Eng. Sci. 66 (23), 6193–6198. https://doi.org/10.1016/j.ces.2011.08.051. https://www.sciencedirect.com/science/article/pii/S0009250911006208.
Bui, M., Gunawan, I., Verheyen, T.V., Meuleman, E., 2016. Dynamic operation of liquid absorbent-based post-combustion CO2capture plants. In: Absorption-Based Post-Combustion Capture of Carbon Dioxide, Woodhead Publishing, pp. 589–621. doi:10.1016/B978-0-08-100514-9.00024-X. https://www.sciencedirect.com/science/article/pii/B978008100514900024X.
Bui, M., Adjiman, C.S., Bardow, A., Anthony, E.J., Boston, A., Brown, S., Fennell, P.S., Fuss, S., Galindo, A., Hackett, L.A., Hallett, J.P., Herzog, H.J., Jackson, G., Kemper, J., Krevor, S., Maitland, G.C., Matuszewski, M., Metcalfe, I.S., Petit, C., Puxty, G., Reimer, J., Reiner, D.M., Rubin, E.S., Scott, S.A., Shah, N., Smit, B., Trusler, J.P.M., Webley, P., Wilcox, J., Mac Dowell, N., 2018. Carbon capture and storage (CCS): the way forward. Energy Environ. Sci. 11 (5), 1062–1176. https://doi.org/10.1039/C7EE02342A.
Caplow, M., 1968. Kinetics of carbamate formation and breakdown. J. Am. Chem. Soc. 90 (24), 6795–6803. https://doi.org/10.1021/ja01026a041. https://pubs.acs.org/sharingguidelines.
Carpenter, A., 2012. CO2 abatement in the iron and steel industry, report CCC/193, Tech. rep., IEA Clean Coal Centre, London, UK.
Chilton, T.H., Colburn, A.P., 1934. Mass transfer (absorption) coefficients: prediction from data on heat transfer and fluid friction. Ind. Eng. Chem. 26 (11), 1183–1187. https://doi.org/10.1021/ie50299a012. https://pubs.acs.org/sharingguidelines.
Couchaux, G., Barth, D., Jacquin, M., Faraj, A., Grandjean, J., 2014. Kinetics of carbon dioxide with amines. I. Stopped-flow studies in aqueous solutions. A review. Oil Gas Sci. Technol. – Rev. IFP Energies nouvelles 69 (5), 865–884. https://doi.org/10.2516/ogst/2013150.
Cousins, A., Cottrell, A., Lawson, A., Huang, S., Feron, P.H.M., 2012 Model verification and evaluation of the rich-split process modification at an Australian-based post combustion CO2 capture pilot plant. In: Greenhouse Gases: Science and Technology, vol. 2, pp. 329–345. doi:10.1002/ghg.1295.
Cousins, A., Nielsen, P., Huang, S., Cottrell, A., Chen, E., Rochelle, G.T., Feron, P.H.M., 2015. Pilot-scale evaluation of concentrated piperazine for CO2 capture at an Australian coal-fired power station: duration experiments. Greenhouse Gases: Sci. Technol. 5 (4), 363–373. https://doi.org/10.1002/ghg.1507. https://onlinelibrary.wiley.com/doi/abs/10.1002/ghg.1507.
Crooks, J.E., Donnellan, J.P., 1989. Kinetics and mechanism of the reaction between carbon dioxide and amines in aqueous solution. J. Chem. Soc. Perkin Trans. 2 (4), 331–333. https://doi.org/10.1039/p29890000331. http://xlink.rsc.org/?DOI=p29890000331.
Danckwerts, P.V., 1979. The reaction of CO2 with ethanolamines. Chem. Eng. Sci. 34 (4), 443–446. https://doi.org/10.1016/0009-2509(79)85087-3. https://www.sciencedirect.com/science/article/pii/0009250979850873.
Darde, V., Van Well, W.J., Stenby, E.H., Thomsen, K., 2010. Modeling of carbon dioxide absorption by aqueous ammonia solutions using the extended UNIQUAC model. Ind. Eng. Chem. Res. 49 (24), 12663–12674. https://doi.org/10.1021/ie1009519. https://pubs.acs.org/doi/10.1021/ie1009519.
Darde, V., van Well, W.J., Fosboel, P.L., Stenby, E.H., Thomsen, K., 2011. Experimental measurement and modeling of the rate of absorption of carbon dioxide by aqueous ammonia. Int. J. Greenhouse Gas Control 5 (5), 1149–1162. https://doi.org/10.1016/j.ijggc.2011.07.008. https://www.sciencedirect.com/science/article/pii/S1750583611001319.
Darde, V., Thomsen, K., van Well, W.J., Bonalumi, D., Valenti, G., Macchi, E., 2012. Comparison of two electrolyte models for the carbon capture with aqueous ammonia. Int. J. Greenhouse Gas Control 8, 61–72. https://doi.org/10.1016/j.ijggc.2012.02.002. https://www.sciencedirect.com/science/article/pii/S1750583612000333.
Da Silva, E.F., Svendsen, H.F., 2004. Ab initio study of the reaction of carbamate formation from CO2 and alkanolamines. Ind. Eng. Chem. Res. 43 (13), 3413–3418. https://doi.org/10.1021/ie030619k. https://pubs.acs.org/sharingguidelines.
Dubois, L., Laribi, S., Mouhoubi, S., De Weireld, G., Thomas, D., 2017. Study of the post-combustion CO2 capture applied to conventional and partial oxy-fuel cement plants. In: Energy Procedia, vol. 114, Elsevier, pp. 6181–6196. doi:10.1016/j.egypro.2017.03.1756. https://www.sciencedirect.com/science/article/pii/S1876610217319586?via%3Dihub.
Freeman, S.A., Dugas, R., Wagener, D.H.V., Nguyen, T., Rochelle, G.T., 2010. Carbon dioxide capture with concentrated, aqueous piperazine. Int. J. Greenhouse Gas Control 4 (2), 119–124. https://doi.org/10.1016/j.ijggc.2009.10.008. https://www.sciencedirect.com/science/article/pii/S1750583609001182.
Froment, G.F., Bischoff, K.B., 1990. Chemical reactor analysis and design, second ed. Edition, Wiley series in chemical engineering, Wiley, New York.
Gardarsdottir, S.O., De Lena, E., Romano, M., Roussanaly, S., Voldsund, M., Pérez-Calvo, J.F., Berstad, D., Fu, C., Anantharaman, R., Sutter, D., Gazzani, M., Mazzotti, M., Cinti, G., 2019. Comparison of technologies for CO 2 capture from cement production—Part 2: Cost analysis. Energies 12 (3), 542. https://doi.org/10.3390/en12030542. http://www.mdpi.com/1996-1073/12/3/542.
Gazzani, M., Romano, M.C., Manzolini, G., 2015. CO2 capture in integrated steelworks by commercial-ready technologies and SEWGS process. Int. J. Greenhouse Gas Control 41, 249–267. https://doi.org/10.1016/j.ijggc.2015.07.012. https://www.sciencedirect.com/science/article/pii/S1750583615300207.
GCCSI, 2017. The Global Status of CCS, Tech. rep., GCCSI. www.globalccsinstitute.com.
Gouedard, C., Picq, D., Launay, F., Carrette, P.L., 2012. Amine degradation in CO 2 capture. I. A review. Int. J. Greenhouse Gas Control 10, 244–270. https://doi.org/10.1016/j.ijggc.2012.06.015. https://www.sciencedirect.com/science/article/pii/S1750583612001508?via%3Dihub.
Hasan, M.M., Baliban, R.C., Elia, J.A., Floudas, C.A., 2012. Modeling, simulation, and optimization of postcombustion CO2 capture for variable feed concentration and flow rate. 1. Chemical absorption and membrane processes. Ind. Eng. Chem. Res. 51 (48), 15642–15664. https://doi.org/10.1021/ie301571d.
Hegerland, G., Pande, J., Haugen, H., Eldrup, N., Tokheim, L.-A., Hatlevik, L., 2006. Capture of CO2 from a cement plant – technical possibilities and economical estimates.
Hills, T., Leeson, D., Florin, N., Fennell, P., 2016. Carbon capture in the cement industry: technologies, progress, and retrofitting. Environ. Sci. Technol. 50 (1), 368–377. https://doi.org/10.1021/acs.est.5b03508.
Ho, M.T., Wiley, D.E., 2016. Liquid absorbent-based post-combustion CO2 capture inindustrial processes. In: Absorption-Based Post-Combustion Capture of Carbon Dioxide, Ch. 28, pp. 711–756. doi:10.1016/B978-0-08-100514-9.00028-7.
Idem, R., Wilson, M., Tontiwachwuthikul, P., Chakma, A., Veawab, A., Aroonwilas, A., Gelowitz, D., 2006. Pilot plant studies of the CO2 capture performance of aqueous MEA and mixed MEA/MDEA solvents at the University of Regina CO2 capture technology development plant and the boundary dam CO2 capture demonstration plant. In: Industrial and Engineering Chemistry Research, vol. 45, pp. 2414–2420. doi:10.1021/ie050569e.
International Energy Agency, 2017. Energy Technology Perspectives 2017 Catalysing Energy Technology Transformations, Tech. rep., International Energy Agency. www.iea.org/etp2017.
International Energy Agency, 2018. Cement Sustainability Initiative, Technology Roadmap – Low-Carbon Transition in the Cement Industry, Tech. rep., International Energy Agency (IEA). www.wbcsdcement.org.
Jänecke, E., 1929a. Über die Löslichkeit von Ammonbicarbonat in Wasser bis zum Schmelzpunkt. Zeitschrift für Elektrochemie 35 (6), 332–334. https://doi.org/10.1002/bbpc.19290350605. https://onlinelibrary.wiley.com/doi/abs/10.1002/bbpc.19290350605 http://onlinelibrary.wiley.com/doi/10.1002/bbpc.19290350605/abstract.
Jänecke, E., 1929b. Über das system H2O, CO2 und NH3. Zeitschrift für Elektrochemie 35 (9), 716–728. https://doi.org/10.1002/bbpc.192900060. https://onlinelibrary.wiley.com/doi/abs/10.1002/bbpc.192900060 http://onlinelibrary.wiley.com/doi/10.1002/bbpc.192900060/abstract.
Jilvero, H., Normann, F., Andersson, K., Johnsson, F., 2014. The rate of CO2 absorption in ammonia-implications on absorber design. Ind. Eng. Chem. Res. 53 (16), 6750–6758. https://doi.org/10.1021/ie403346a.
Kale, C., Górak, A., Schoenmakers, H., 2013. Modelling of the reactive absorption of CO2 using mono-ethanolamine. Int. J. Greenhouse Gas Control 17, 294–308. https://doi.org/10.1016/j.ijggc.2013.05.019. https://www.sciencedirect.com/science/article/pii/S1750583613002351.
Kentish, S.E., 2016. Reclaiming of amine-based absorption liquids used in post-combustion capture. In: Absorption-Based Post-Combustion Capture of Carbon Dioxide. Woodhead Publishing, pp. 426–438. doi:10.1016/B978-0-08-100514-9.00017-2. https://www.sciencedirect.com/science/article/pii/B9780081005149000172.
Kim, G.H., Park, S.Y., You, J.K., Hong, W.H., Kim, J.N., Kim, J.D., 2014. CO2 absorption kinetics in a CO2-free and partially loaded aqueous ammonia solution. Chem. Eng. J. 250, 83–90. https://doi.org/10.1016/j.cej.2014.03.120. https://www.sciencedirect.com/science/article/pii/S1385894714004203#f0005.
Kucka, L., Kenig, E.Y., Górak, A., 2002. Kinetics of the gas-liquid reaction between carbon dioxide and hydroxide ions. Ind. Eng. Chem. Res. 41 (24), 5952–5957. https://doi.org/10.1021/ie020452f.
Kuramochi, T., Ramírez, A., Turkenburg, W., Faaij, A., 2012. Comparative assessment of CO2 capture technologies for carbon-intensive industrial processes. Prog. Energy Combust. Sci. 38 (1), 87–112. https://doi.org/10.1016/j.pecs.2011.05.001. https://www.sciencedirect.com/science/article/pii/S0360128511000293.
Kwak, N.S., Lee, J.H., Lee, I.Y., Jang, K.R., Shim, J.G., 2012. A study of the CO2 capture pilot plant by amine absorption. Energy 47 (1), 41–46. https://doi.org/10.1016/j.energy.2012.07.016. https://www.sciencedirect.com/science/article/pii/S0360544212005464.

Laribi, S., Dubois, L., De Weireld, G., Thomas, D., 2019. Study of the post-combustion CO2 capture process by absorption-regeneration using amine solvents applied to cement plant flue gases with high CO2 contents. Int. J. Greenhouse Gas Control 90, 102799. https://doi.org/10.1016/j.ijggc.2019.102799. https://www.sciencedirect.com/science/article/pii/S1750583619300660.

Leeson, D., Mac Dowell, N., Shah, N., Petit, C., Fennell, P.S., 2017. A Techno-economic analysis and systematic review of carbon capture and storage (CCS) applied to the iron and steel, cement, oil refining and pulp and paper industries, as well as other high purity sources. Int. J. Greenhouse Gas Control 61, 71–84. https://doi.org/10.1016/j.ijggc.2017.03.020. https://www.sciencedirect.com/science/article/pii/S175058361730289X.

Lemaire, E., Bouillon, P.A., Lettat, K., 2014. Developpement du procede hicaptpour le captage du co2: Du laboratoire au pilote industriel. Oil Gas Sci. Technol. 69 (6), 1069–1080. https://doi.org/10.2516/ogst/2013153. http://ogst.ifpenergiesnouvelles.fr/10.2516/ogst/2013153.

Levenspiel, O., 1999. Fluid-fluid reactions: kinetics. In: Chemical reaction engineering, third ed. Wiley, New York, Ch. 23.

Liebenthal, U., Di, D., Pinto, D., Monteiro, J.G., Svendsen, H.F., Kather, A., 2013. Overall process analysis and optimisation for CO2 Capture from coal fired power plants based on phase change solvents forming two liquid phases. In: Energy Procedia, vol. 37, Elsevier, pp. 1844–1854. doi:10.1016/j.egypro.2013.06.064. https://www.sciencedirect.com/science/article/pii/S187661021300307X.

Li, B.H., Zhang, N., Smith, R., 2016. Simulation and analysis of CO2 capture process with aqueous monoethanolamine solution. Appl. Energy 161, 707–717. https://doi.org/10.1016/j.apenergy.2015.07.010. https://www.sciencedirect.com/science/article/pii/S0306261915008399.

Lillia, S., Bonalumi, D., Fosbøl, P.L., Thomsen, K., Valenti, G., 2018. Experimental study of the aqueous CO2-NH3 rate of reaction for temperatures from 15 °C to 35 °C, NH3 concentrations from 5% to 15% and CO2 loadings from 0.2 to 0.6. Int. J. Greenhouse Gas Control 70, 117–127. https://doi.org/10.1016/j.ijggc.2018.01.009. https://www.sciencedirect.com/science/article/pii/S1750583617306576?via%3Dihub.

Lin, Y.J., Madan, T., Rochelle, G.T., 2014. Regeneration with rich bypass of aqueous piperazine and monoethanolamine for CO2 capture. Ind. Eng. Chem. Res. 53 (10), 4067–4074. https://doi.org/10.1021/ie403750s.

Liu, J., Gao, H.C., Peng, C.C., Wong, D.S.H., Jang, S.S., Shen, J.F., 2015. Aspen Plus rate-based modeling for reconciling laboratory scale and pilot scale CO2 absorption using aqueous ammonia. Int. J. Greenhouse Gas Control 34, 117–128. https://doi.org/10.1016/j.ijggc.2015.01.009. https://www.sciencedirect.com/science/article/pii/S1750583615000250.

Lombardo, G., Agarwal, R., Askander, J., 2014. Chilled ammonia process at technology center Mongstad-first results. In: Energy Procedia, vol. 51, pp. 31–39. doi:10.1016/j.egypro.2014.07.004. www.sciencedirect.com.

Luo, X., Wang, M., 2017. Improving prediction accuracy of a rate-based model of an MEA-based carbon capture process for large-scale commercial deployment. Engineering 3 (2), 232–243. https://doi.org/10.1016/J.ENG.2017.02.001. https://www.sciencedirect.com/science/article/pii/S209580991730303X.

Mangalapally, H.P., Hasse, H., 2011. Pilot plant study of post-combustion carbon dioxide capture by reactive absorption: Methodology, comparison of different structured packings, and comprehensive results for monoethanolamine. Chem. Eng. Res. Des. 89 (8), 1216–1228. https://doi.org/10.1016/j.cherd.2011.01.013. https://www.sciencedirect.com/science/article/pii/S0263876211000396.

Mangalapally, H.P., Notz, R., Asprion, N., Sieder, G., Garcia, H., Hasse, H., 2012. Pilot plant study of four new solvents for post combustion carbon dioxide capture by reactive absorption and comparison to MEA. Int. J. Greenhouse Gas Control 8 (22), 205–216. https://doi.org/10.1016/j.ijggc.2012.02.014. https://www.sciencedirect.com/science/article/pii/S0009250911004404.

Manzolini, G., Macchi, E., Binotti, M., Gazzani, M., 2011. Integration of SEWGS for carbon capture in Natural Gas Combined Cycle. Part B: Reference case comparison. Int. J. Greenhouse Gas Control 5 (2), 214–225. https://doi.org/10.1016/j.ijggc.2010.08.007. https://www.sciencedirect.com/science/article/pii/S1750583610001350.

Masel, R.I., 2001. Chemical Kinetics and Catalysis. J. Wiley, New York.

Mazari, S.A., Si Ali, B., Jan, B.M., Saeed, I.M., Nizamuddin, S., 2015. An overview of solvent management and emissions of amine-based CO2 capture technology. Int. J. Greenhouse Gas Control 34, 129–140. https://doi.org/10.1016/j.ijggc.2014.12.017. https://www.sciencedirect.com/science/article/pii/S175058361400396X?via%3Dihub.

Meuleman, E., Cottrell, A., Ghayur, A., 2016. Treatment of flue-gas impurities for liquid absorbent-based post-combustion CO2 capture processes. In: Absorption-Based Post-Combustion Capture of Carbon Dioxide, Woodhead Publishing, pp. 519–551. doi:10.1016/B978-0-08-100514-9.00022-6. https://www.sciencedirect.com/science/article/pii/B9780081005149000226.

Nguyen, T., Hilliard, M., Rochelle, G.T., 2010. Amine volatility in CO2 capture. Int. J. Greenhouse Gas Control 4 (5), 707–715. https://doi.org/10.1016/j.ijggc.2010.06.003. https://www.sciencedirect.com/science/article/pii/S1750583610001003.

Notz, R., Mangalapally, H.P., Hasse, H., 2012. Post combustion CO2 capture by reactive absorption: Pilot plant description and results of systematic studies with MEA. Int. J. Greenhouse Gas Control 6, 84–112. https://doi.org/10.1016/j.ijggc.2011.11.004. https://www.sciencedirect.com/science/article/pii/S1750583611002143.

Nwaoha, C., Supap, T., Idem, R., Saiwan, C., Tontiwachwuthikul, P., AL-Marri, M.J., Benamor, A., 2017. Advancement and new perspectives of using formulated reactive amine blends for post-combustion carbon dioxide (CO2) capture technologies. Petroleum 3 (1), 10–36. https://doi.org/10.1016/J.PETLM.2016.11.002. https://www.sciencedirect.com/science/article/pii/S2405656116301808.

Onda, K., Takeuchi, H., Okumoto, Y., 1968. Mass transfer coefficients between gas and liquid phases in packed columns. J. Chem. Eng. Jpn. 1 (1), 56–62. https://doi.org/10.1252/jcej.1.56.

Petra Nova, 2020, W.A. Parish Project — Department of Energy. https://www.energy.gov/fe/petra-nova-wa-parish-project https://energy.gov/fe/petra-nova-wa-parish-project.

Pinsent, B.R., Pearson, L., Roughton, F.J., 1956a. The kinetics of combination of carbon dioxide with ammonia. Trans. Faraday Soc. 52, 1594–1598. https://doi.org/10.1039/tf9565201512.

Pinsent, B.R., Pearson, L., Roughton, F.J., 1956b. The kinetics of combination of carbon dioxide with hydroxide ions. Trans. Faraday Soc. 52, 1512–1520. https://doi.org/10.1039/tf9565201512. http://xlink.rsc.org/?DOI=tf9565201594.

Psarras, P.C., Comello, S., Bains, P., Charoensawadpong, P., Reichelstein, S., Wilcox, J., 2017. Carbon capture and utilization in the industrial sector. Environ. Sci. Technol. 51 (19), 11440–11449. https://doi.org/10.1021/acs.est.7b01723.

Puxty, G., Maeder, M., 2016. The fundamentals of post-combustion capture. In: Absorption-Based Post-Combustion Capture of Carbon Dioxide, Woodhead Publishing, pp. 13–33. doi:10.1016/B978-0-08-100514-9.00002-0. https://www.sciencedirect.com/science/article/pii/B9780081005149000020.

Qi, G., Wang, S., Yu, H., Wardhaugh, L., Feron, P., Chen, C., 2013. Development of a rate-based model for CO2 absorption using aqueous NH3 in a packed column. Int. J. Greenhouse Gas Control 17, 450–461. https://doi.org/10.1016/j.ijggc.2013.05.027. https://www.sciencedirect.com/science/article/pii/S1750583613002430.

Que, H., Chen, C.C., 2011. Thermodynamic modeling of the NH 3-CO 2-H 2O system with electrolyte NRTL model. Ind. Eng. Chem. Res. 50 (19), 11406–11421. https://doi.org/10.1021/ie201276m. https://pubs.acs.org/doi/10.1021/ie201276m.

Rabensteiner, M., Kinger, G., Koller, M., Gronald, G., Hochenauer, C., 2014a. Pilot plant study of ethylenediamine as a solvent for post combustion carbon dioxide capture and comparison to monoethanolamine. Int. J. Greenhouse Gas Control 27, 1–14. https://doi.org/10.1016/j.ijggc.2014.05.002. https://www.sciencedirect.com/science/article/pii/S175058361400125X.

Rabensteiner, M., Kinger, G., Koller, M., Gronald, G., Unterberger, S., Hochenauer, C., 2014b. Investigation of the suitability of aqueous sodium glycinate as a solvent for post combustion carbon dioxide capture on the basis of pilot plant studies and screening methods. Int. J. Greenhouse Gas Control 29, 1–15. https://doi.org/10.1016/j.ijggc.2014.07.011. https://www.sciencedirect.com/science/article/pii/S1750583614002102.

Rabensteiner, M., Kinger, G., Koller, M., Hochenauer, C., 2015. PCC pilot plant studies with aqueous potassium glycinate. Int. J. Greenhouse Gas Control 42, 562–570. https://doi.org/10.1016/j.ijggc.2015.09.012. https://www.sciencedirect.com/science/article/pii/S1750583615300797.

Rabensteiner, M., Kinger, G., Koller, M., Hochenauer, C., 2016. Pilot plant study of aqueous solution of piperazine activated 2-amino-2-methyl-1-propanol for post combustion carbon dioxide capture. Int. J. Greenhouse Gas Control 51, 106–117. https://doi.org/10.1016/j.ijggc.2016.04.035. https://www.sciencedirect.com/science/article/pii/S1750583616302225.

Raynal, L., Alix, P., Bouillon, P.A., Gomez, A., Le Febvre De Nailly, M., Jacquin, M., Kittel, J., Di Lella, A., Mougin, P., Trapy, J., 2011. The DMX process: An original solution for lowering the cost of post-combustion carbon capture. In: Energy Procedia, vol. 4, Elsevier, pp. 779–786. doi:10.1016/j.egypro.2011.01.119. https://www.sciencedirect.com/science/article/pii/S1876610211001214.

Reynolds, A.J., Verheyen, T.V., Meuleman, E., 2016. Degradation of amine-based solvents. In: Absorption-Based Post-Combustion Capture of Carbon Dioxide. Woodhead Publishing, pp. 399–423. doi:10.1016/B978-0-08-100514-9.00016-0. https://www.sciencedirect.com/science/article/pii/B9780081005149000160.

Rochelle, G.T., 2016. Conventional amine scrubbing for CO 2 capture. In: Absorption-Based Post-Combustion Capture of Carbon Dioxide, Ch. 3, pp. 35–67. doi:10.1016/B978-0-08-100514-9.00003-2.

Rochelle, G.T., Wu, Y., Chen, E., Akinpelumi, K., Fischer, K.B., Gao, T., Liu, C.-T., Selinger, J.L., 2019. Pilot plant demonstration of piperazine with the advanced flash stripper. Int. J. Greenhouse Gas Control 84, 72–81. https://doi.org/10.1016/j.ijggc.2019.03.014. https://linkinghub.elsevier.com/retrieve/pii/S1750583618307485.

D. Sachde, G.T. Rochelle, Absorber intercooling configurations using aqueous piperazine for capture from sources with 4 to 27% CO2. In: Energy Procedia, vol. 63, Elsevier, pp. 1637–1656. doi:10.1016/j.egypro.2014.11.174. https://www.sciencedirect.com/science/article/pii/S1876610214019894.

Sakwattanapong, R., Aroonwilas, A., Veawab, A., 2005. Behavior of reboiler heat duty for CO2 capture plants using regenerable single and blended alkanolamines. Ind. Eng. Chem. Res. 44 (12), 4465–4473. https://doi.org/10.1021/ie050063w.

Smith, K., Xiao, G., Mumford, K., Gouw, J., Indrawan, I., Thanumurthy, N., Quyn, D., Cuthbertson, R., Rayer, A., Nicholas, N., Lee, A., Da Silva, G., Kentish, S., Harkin, T., Qader, A., Anderson, C., Hooper, B., Stevens, G., 2014. Demonstration of a concentrated potassium carbonate process for CO2 capture. In: Energy and Fuels, vol. 28, pp. 299–306. doi:10.1021/ef4014746.

Stec, M., Tatarczuk, A., Wikecław-Solny, L., Krótki, A., Spietz, T., Wilk, A., Śpiewak, D., 2016. Demonstration of a post-combustion carbon capture pilot plant using amine-based solvents at the Łaziska Power Plant in Poland. Clean Technol. Environ. Policy 18 (1), 151–160. https://doi.org/10.1007/s10098-015-1001-2.

Stichlmair, J., Bravo, J.L., Fair, J.R., 1989. General model for prediction of pressure drop and capacity of countercurrent gas/liquid packed columns. Gas Sep. Purif.

3 (1), 19–28. https://doi.org/10.1016/0950-4214(89)80016-7. https://www.sciencedirect.com/science/article/pii/0950421489800167.

Sutter, D., Gazzani, M., Mazzotti, M., 2015. Formation of solids in ammonia-based CO2 capture processes — identification of criticalities through thermodynamic analysis of the CO2–NH3–H2O system. Chem. Eng. Sci. 133, 170–180. https://doi.org/10.1016/j.ces.2014.12.064. https://www.sciencedirect.com/science/article/pii/S0009250915000160.

Sutter, D., Gazzani, M., Mazzotti, M., 2016. A low-energy chilled ammonia process exploiting controlled solid formation for post-combustion CO2 capture. Faraday Discuss. 192, 59–83. https://doi.org/10.1039/C6FD00044D.

Telikapalli, V., Kozak, F., Leandri, J.F., Sherrick, B., Black, J., Muraskin, D., Cage, M., Hammond, M., Spitznogle, G., 2011. CCS with the alstom chilled ammonia process development program- Field pilot results. In: Energy Procedia, vol. 4, Elsevier, pp. 273–281. doi:10.1016/j.egypro.2011.01.052. https://www.sciencedirect.com/science/article/pii/S1876610211000531.

Thomsen, K., Rasmussen, P., 1999. Modeling of vapor-liquid-solid equilibrium in gas-aqueous electrolyte systems. Chem. Eng. Sci. 54 (12), 1787–1802. https://doi.org/10.1016/S0009-2509(99)00019-6. https://www.sciencedirect.com/science/article/pii/S0009250999000196.

Tobiesen, F.A., Svendsen, H.F., Mejdell, T., 2007. Modeling of blast furnace CO2 capture using amine absorbents. Ind. Eng. Chem. Res. 46 (23), 7811–7819. https://doi.org/10.1021/ie061556j.

Tsay, C., Pattison, R.C., Zhang, Y., Rochelle, G.T., Baldea, M., 2019. Rate-based modeling and economic optimization of next-generation amine-based carbon capture plants. Appl. Energy 252, 113379. https://doi.org/10.1016/j.apenergy.2019.113379. https://linkinghub.elsevier.com/retrieve/pii/S0306261919310530.

Vaidya, P.D., Kenig, E.Y., 2007. Gas-liquid reaction kinetics: A review of determination methods. doi:10.1080/00986440701518314. http://www.tandfonline.com/doi/abs/10.1080/00986440701518314.

van der Spek, M., Roussanaly, S., Rubin, E.S., 2019. Best practices and recent advances in CCS cost engineering and economic analysis. Int. J. Greenhouse Gas Control 83, 91–104. https://doi.org/10.1016/j.ijggc.2019.02.006. https://www.sciencedirect.com/science/article/pii/S175058361930101X https://linkinghub.elsevier.com/retrieve/pii/S175058361930101X.

Voldsund, M., Gardarsdottir, S., De Lena, E., Pérez-Calvo, J.-F., Jamali, A., Berstad, D., Fu, C., Romano, M., Roussanaly, S., Anantharaman, R., Hoppe, H., Sutter, D., Mazzotti, M., Gazzani, M., Cinti, G., Jordal, K., 2019. Comparison of technologies for CO2 capture from cement production—Part 1: Technical evaluation. Energies 12 (3), 559. https://doi.org/10.3390/en12030559. http://www.mdpi.com/1996-1073/12/3/559.

Wang, X., Conway, W., Fernandes, D., Lawrance, G., Burns, R., Puxty, G., Maeder, M., 2011. Kinetics of the reversible reaction of CO2(aq) with ammonia in aqueous solution. J. Phys. Chem. A 115 (24), 6405–6412. https://doi.org/10.1021/jp108491a. https://pubs.acs.org/sharingguidelines.

Yu, J., Wang, S., 2015. Development of a novel process for aqueous ammonia based CO_2 capture. Int. J. Greenhouse Gas Control 39, 129–138. https://doi.org/10.1016/j.ijggc.2015.05.008. https://www.sciencedirect.com/science/article/pii/S1750583615001711.

Yu, H., Morgan, S., Allport, A., Cottrell, A., Do, T., McGregor, J., Wardhaugh, L., Feron, P., 2011. Results from trialling aqueous NH3 based post-combustion capture in a pilot plant at Munmorah power station: Absorption. Chem. Eng. Res. Des. 89 (8), 1204–1215. https://doi.org/10.1016/J.CHERD.2011.02.036. https://www.sciencedirect.com/science/article/pii/S0263876211001079?via%3Dihub.

Yu, H., Tan, Z., Thé, J., Feng, X., Croiset, E., Anderson, W.A., 2016. Kinetics of the absorption of carbon dioxide into aqueous ammonia solutions. AIChE J. 62 (10), 3673–3684. https://doi.org/10.1002/aic.15296.

Zhang, M.S.J., 2013. Study on CO 2 Capture Using Thermomorphic Biphasic Solvents with Energy-Efficient Regeneration Zur Erlangung des akademischen Grades eines, Ph.D. thesis, TU Dortmund.

Zhang, Y., Chen, C.-C., 2013. Modeling CO2 absorption and desorption by aqueous monoethanolamine solution with aspen rate-based model. Energy Procedia 37, 1584–1596. https://doi.org/10.1016/j.egypro.2013.06.034. http://www.sciencedirect.com/science/article/pii/S1876610213002774.

Zhang, Y., Chen, H., Chen, C.C., Plaza, J.M., Dugas, R., Rochelle, G.T., 2009. Rate-based process modeling study of CO2 Capture with aqueous monoethanolamine solution. Ind. Eng. Chem. Res. 48 (20), 9233–9246. https://doi.org/10.1021/ie900068k. https://pubs.acs.org/doi/10.1021/ie900068k.